Inorganic Chemistry Article
Cite This: Inorg. Chem. 2020, 59, 1075−1090
pubs.acs.org/IC

Advanced Paramagnetic Resonance Studies on Manganese and Iron Corroles with a Formal d^4 Electron Count

J. Krzystek,[†] Alexander Schnegg,[‡,§] Azar Aliabadi,[§] Karsten Holldack,[∥] Sebastian A. Stoian,[⊥] Andrew Ozarowski,[†] Scott D. Hicks,[#] Mahdi M. Abu-Omar,[¶] Kolle E. Thomas,[□] Abhik Ghosh,[□] Kenneth P. Caulfield,[○] Zachary J. Tonzetich,[○] and Joshua Telser*,[△]

[†] National High Magnetic Field Laboratory, Florida State University, Tallahassee, Florida 32310, United States

[‡] EPR Research Group, Max Planck Institute for Chemical Energy Conversion, Stiftstraße 34-36, D-45470 Mülheim Ruhr, Germany

[§] Berlin Joint EPR Laboratory, Helmholtz-Zentrum Berlin, Kekulestraße 5, D-12489 Berlin, Germany

[∥] Institut für Methoden und Instrumentierung der Forschung mit Synchrotronstrahlung am Elektronenspeicherring BESSY II, Albert-Einstein-Straße 15, D-12489 Berlin, Germany

[⊥] Department of Chemistry, University of Idaho, Moscow, Idaho 83844, United States

[#] Department of Chemistry, Purdue University, West Lafayette, Indiana 47907, United States

[¶] Departments of Chemistry and Biochemistry, University of California, Santa Barbara, California 93106-9510, United States

[□] Department of Chemistry, UiT−The Arctic University of Norway, N-9037 Tromsø, Norway

[○] Department of Chemistry, University of Texas at San Antonio (UTSA), One UTSA Circle, San Antonio, Texas 78249, United States

[△] Department of Biological, Physical, and Health Sciences, Roosevelt University, Chicago, Illinois 60605, United States

* Supporting Information

ABSTRACT: Metallocorroles wherein the metal ion is Mn^{III} and formally Fe^{IV} are studied here using field- and frequency-domain electron paramagnetic resonance techniques. The Mn^{III} corrole, Mn(tpfc) (tpfc = 5,10,15-tris(pentafluorophenyl)corrole trianion), exhibits the following S = 2 zero-field splitting (zfs) parameters: D = −2.67(1) cm^{-1}, |E| = 0.023(5) cm^{-1}. This result and those for other Mn^{III} tetrapyrroles indicate that when D ≈− 2.5 ± 0.5 cm^{-1} for 4- or 5coordinate and D ≈− 3.5 ± 0.5 cm^{-1} for 6-coordinate complexes, the ground state description is $[Mn^{III}(Cor^{3-})]^0$ or $[Mn^{III}(P^{2-})]^+$ (Cor = corrole, P = porphyrin). The situation for formally Fe^{IV} corroles is more complicated, and it has been shown that for Fe(Cor)X, when X = Ph (phenyl), the ground state is a spin triplet best described by $[Fe^{IV}(Cor^{3-})]^+$, but when X = halide, the ground state corresponds to $[Fe^{III}(Cor^{\bullet 2-})]^+$, wherein an intermediate spin (S = $^3/_2$) Fe^{III} is antiferromagnetically coupled to a corrole radical dianion (S = $^1/_2$) to also give an S = 1 ground state. These two valence isomers can be distinguished by their zfs parameters, as determined here for Fe(tpc)X, X = Ph, Cl (tpc = 5,10,15triphenylcorrole trianion). The complex with axial phenyl gives D = 21.1(2) cm^{-1}, while that with axial chloride gives D = 14.6(1) cm^{-1}. The D value for Fe(tpc)Ph is in rough agreement with the range of values reported for other Fe^{IV} complexes. In contrast, the D value for Fe(tpc)Cl is inconsistent with an Fe^{IV} description and represents a different type of iron center. Computational studies corroborate the zfs for the two types of iron corrole complexes. Thus, the zfs of metallocorroles can be diagnostic as to the electronic structure of a formally high oxidation state metallocorrole, and by extension to metalloporphyrins, although such studies have yet to be performed.

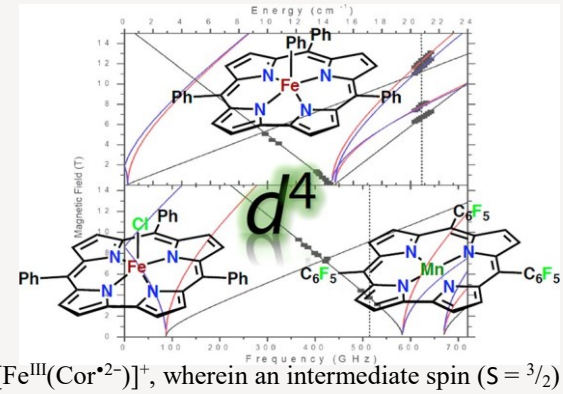

DOI: 10.1021/acs.inorgchem.9b02635
Inorg. Chem. 2020, 59, 1075−1090

INTRODUCTION

Among the many types of tetrapyrrole ligands, corroles are of particular interest because of their ability to engender formally high-oxidation-state transition metal complexes.[1−8] The key qualifier in the foregoing sentence is "formally", as corroles are also paradigms for the phenomenon of "ligand noninnocence".[9] Among the vast number of corrole derivatives, iron

corroles are of particular interest as models for high-oxidation state intermediates of heme and nonheme iron proteins. An important question regarding all these species concerns the location of the oxidizing equivalent(s) beyond the "standard"

Received: September 2, 2019 Published: January 7, 2020

Scheme 1. Chemical Structure Diagrams of the Three Complexes Studied Spectroscopically Here: Fe(tpc)Cl, Fe(tpc)Ph (Left), and Mn(tpfc) (Right)

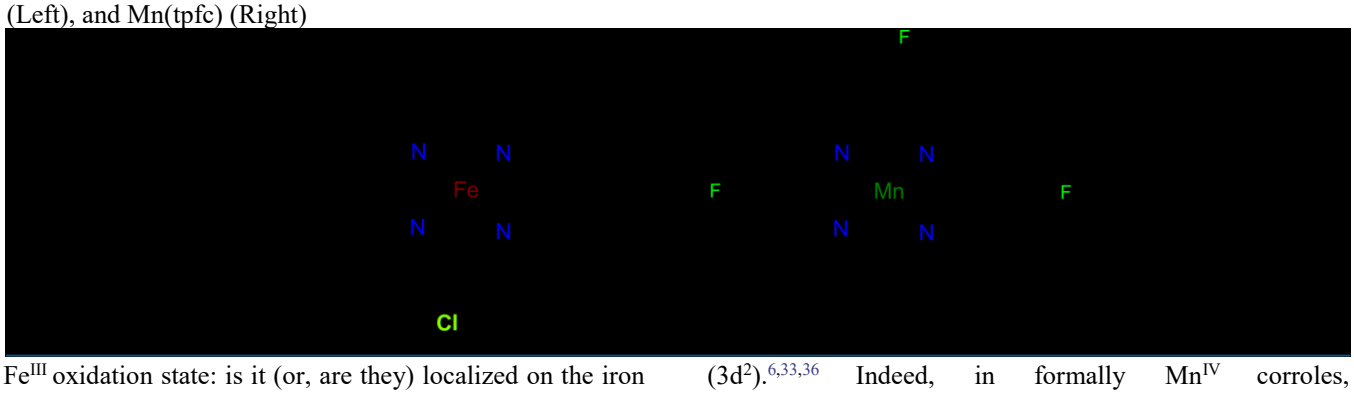

Fe^{III} oxidation state: is it (or, are they) localized on the iron or partly or fully delocalized to the porphyrin, corrole, or other ligand?[8,10] For example, cytochrome P450 Compound I is best described as Fe^{IV} with a delocalized porphyrin-thiyl radical rather than as Fe^{V}.[11] Similar "noninnocent" descriptions apply to other Compounds I in heme oxidases such as horseradish peroxidase (HRP)[12] and chloroperoxidase (CPO)[13] and in various model compounds for these enzymes.[14−16] For Fe corrole complexes Fe(Cor)X (Cor = generic corrole macrocycle; X = monoanionic ligand such as halide), the electronic structure varies from $S = 1$ Fe^{IV} with a corrole(3−) ligand to intermediate-spin $S = {}^{3}/_{2}$ Fe^{III} antiferromagnetically coupled to a corrole(•2−) radical ligand to generate a net spin triplet ($S = 1$).[17−22] These electronic-structural variations lead to distinct experimental signatures, vis-a-vis ^{1}H NMR, optical, and X-ray absorption spectroscopies, subtle bond length alternations in the corrole macrocycle, and electrochemistry.[10] For $S > {}^{1}/_{2}$ complexes such as these, another important electronicstructural probe is provided by their zero-field splitting (zfs),[23,24] usually given by the axial parameter D and the rhombic parameter, E. These parameters can be definitively extracted by electron paramagnetic resonance (EPR) spectroscopy in both the field domain (using high frequencies and fields, HFEPR),[25−27] and in the frequency domain (FD-FT THz-EPR),[28,29] as well as by other techniques.[30] We describe here the use of both of these paramagnetic resonance techniques to extract the complete spin Hamiltonian parameters of two 5-coordinate formally Fe^{IV} corrole complexes, which have spin triplet ground states: Fe(tpc)Ph and Fe(tpc)Cl (tpc = 5,10,15-triphenylcorrole trianion; Ph = phenyl).[31] The structures of these compounds are shown in Scheme 1 (left). The structures of other relevant tetrapyrrole complexes are shown in Scheme S1 and of other macrocyclic complexes of background interest are shown in Scheme S2 (both in the Supporting Information).

For comparison, we also present HFEPR results on a Mn^{III} corrole, Mn(tpfc) (tpfc = 5,10,15-tris(pentafluorophenyl)corrole trianion; Scheme 1, right).[6,32,33] As described above for iron, corrole complexes of manganese are also of inherent interest,[34] especially in higher formal oxidation states such as Mn^{IV} ($3d^3$)[35] and Mn^{V} ($3d^2$).[6,33,36] Indeed, in formally Mn^{IV} corroles, electrochemistry and optical spectroscopy,[18,19] and later XANES and computational studies,[35] demonstrated that these are best described as $[Mn^{III}(Cor^{\bullet 2-})]^{+}$. However, in the Mn $3d^4$ situation, unlike with either the same element as in Mn^{IV} or the same formal d electron count as in Fe^{IV}, there is no ambiguity in the description of Mn^{III} corrole complexes in terms of their ground state (i.e., that which one obtains at low temperature, $T < 10$ K ≈ 7 cm^{-1}). At low temperature,[37] trivalent manganese corroles are best described as a metal trication with a corrole trianionic macrocyclic ligand, thus Mn^{III} in its high-spin ($S = 2$) ground state. Accordingly, the Mn(tpfc) zfs results act as a "control" for comparison with the zfs determined for the two different formally Fe^{IV} corrole complexes. The zfs of Mn(tpfc) is also of interest in its own right as a large number of porphyrin (i.e., formally dianionic) complexes of Mn^{III} have been investigated by HFEPR,[25,38−42] even in a protein environment,[43] as well as by other techniques,[44−46] but such studies on corroles are relatively few.[47,48] Moreover, of the two lone prior investigations of Mn^{III} corroles by HFEPR, that by Licoccia and coworkers involved a differently substituted corrole macrocycle (dehmc = 8,12diethyl-2,3,7,13,17,18-hexamethylcorrole),[48] and the

DOI: 10.1021/acs.inorgchem.9b02635
Inorg. Chem. 2020, 59, 1075−1090

study by Bendix et al., although on a tpfc complex,[47] comprised a Mn(III) center bearing an axial triphenylphosphine oxide ligand, i.e., Mn(tpfc)($OPPh_3$), and thus exhibited approximate square pyramidal geometry rather than square planar. Furthermore, Licoccia and coworkers investigated the HFEPR of their corrole complex in a highly concentrated (~0.2 M) frozen solution of pyridine,[48] where axial coordination by solvent to give monopyridine or perhaps even bis-pyridine adducts is likely. The present study is thus the first to investigate by HFEPR an unequivocally square planar Mn^{III} corrole complex in dilute (~1 mM) frozen solution of a noncoordinating solvent, benzene.

The electronic structures of the three formally d^4 complexes shown in Scheme 1 are quite different, as reflected in the magnitude of their zfs. This difference is a consequence of the metallocorrole unit in Fe(tpc)Ph being best described as $[Fe^{IV}(tpc^{3-})]^+$, while Fe(tpc)Cl is more accurately given as $[Fe^{III}(tpc^{\bullet 2-})]^+$.[10] This difference is depicted qualitatively in Scheme 2, which is also applicable to Mn corroles with
$[Mn^{III}(tpfc^{3-})]^0$ being the operative description.

These results will also be related to studies on Fe corroles that address the question of valence description using other experimental techniques (e.g., optical and X-ray absorption spectroscopies)[10] and applied-field Mössbauer spectroscopy.[20,21] Structural aspects of metallocorroles have been summarized in detail by Thomas et al.,[3] but we note that no X-ray crystallographic structures have been reported for Fe(tpc)X (X = Cl, Ph) but have been reported for two close analogues, namely Fe(tmc)Cl (tmc = 5,10,15-trimesitylcorrole trianion; CSD code: ATIXEH),[49] and Fe(tpfc)Cl (CSD code: MELBOU),[50] and one analogue of Fe(tpc)Ph, namely
Fe(ttc)Ph (ttc = 5,10,15-tris(4-methylphenyl)lcorrole trianion (= tritolylcorrole); CSD code POGWEP).[51] The structures of Scheme 2. Qualitative MO Scheme Showing the Difference between $[Fe^{IV}(Cor^{3-})]^+$, Comprised of a Tetragonal Fe^{IV} with S = 1 (Left) and $[Fe^{III}(Cor^{2-\bullet})]^+$, Comprised of an Intermediate Spin Fe^{III} (S = $^3/_2$) Antiferromagnetically
Coupled to a Corrole Dianion Radical to Give a Total Spin S = 1[a]

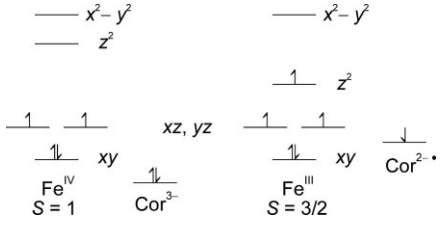

[a]This scheme is also applicable to manganese: $[Mn^{III}(Cor^{3-})]^0$ (left) and $[Mn^{II}(Cor^{2-\bullet})]^0$ (right).

two relevant metallocorroles with alkyl substituents on the pyrroles have also been determined: Fe(oec)Cl (oec = 2,3,7,8,12,13,17,18-octaethylcorrole trianion ; CSD code: SUMWUS) and Fe(oec)Ph (CSD code SUMXED).[52]

EXPERIMENTAL SECTION

Synthesis. The complexes Mn(tpfc),[6] Fe(tpc)Cl,[53] and Fe(tpc)Ph[10] were prepared as previously described.

Mössbauer. Mössbauer spectra were recorded in zero-applied field for neat powder samples of Fe(tpc)Cl (50 mg) and Fe(tpc)Ph (30 mg) at room temperature and at 130 K. These spectra were obtained using a spectrometer operated in constant acceleration mode equipped with a liquid nitrogen-cooled cryostat. The isomer shifts are reported with respect to the center of a spectrum recorded for an α-Fe metal foil at room temperature. Reported spectral parameters were derived from simulations obtained using the WMOSS software (See Co. formerly Web Research Co., Medina, MN).

HFEPR. HFEPR experiments were performed using the previously described spectrometer,[54] which was modified with a Virginia Diodes (Charlottesville, VA) source operating at either 13 ± 1 or 15.5 ± 3 GHz and generating frequencies between 48 and 648 GHz by a cascade of multipliers. The sample was either a solution in benzene in the case of Mn(tpfc) (~1 mM) or a pure microcrystalline solid pressed into a pellet to avoid field-torquing effects in case of the Fe(IV) corroles. Benzene, unlike toluene, is not a traditionally desirable EPR solvent, as it is not glassing. However, we found that in HFEPR, in contrast to conventional EPR, high quality glasses are not necessary. The high melting point of benzene helped ensure rapid freezing of the solution and eliminate the possibility of any solute precipitation. The medium stabilizing the pellet was n-eicosane.

HFEPR spectra were simulated using the program SPIN (by A. Ozarowski), which employs a standard spin Hamiltonian for S > 1/2 systems:[55]

$$H = \beta_e \mathbf{B} g S\, D\, S + (\, {}_z^2 - \_^1 3S\, S(\, + +1))\, E\, S(\, {}_x^2 - S_y^2) \qquad (1)$$

FD-FT THz-EPR. Frequency domain Fourier transform THz-EPR (FD-FT THz-EPR) measurements on pressed pellets Fe(tpc)Cl (28 mg, with 41 mg polyethylene (PE) powder) and Fe(tpc)Ph (27 mg, with 67 mg PE powder) were performed at selected temperatures and external magnetic fields using the low-α radiation from the BESSY II synchrotron in combination with a pumped He cooled Si bolometer detector as described elsewhere.[28,29] A 50 μm Mylar beamsplitter was used. This configuration is most sensitive in the energy range from 7 to 30 cm^{-1}. Experimental resolution was at least 0.5 cm^{-1}.

Absolute EPR-induced THz transmission changes as the ratio of the sample spectrum to a reference. The latter can be either the empty-cryostat spectrum or a spectrum taken on the same sample, albeit at a different temperature or external magnetic field. By dividing spectra taken at low temperature by spectra taken at elevated temperature, changes in the population of the spin energy levels may be recorded as EPR induced transmission changes (FD-FT THz-EPR absorption spectrum). This method can be used even without external magnetic field. However, many nonmagnetic absorption processes also depend on temperature and are sometimes difficult to distinguish from spin (EPR) transitions.

DOI: 10.1021/acs.inorgchem.9b02635
Inorg. Chem. 2020, 59, 1075−1090

Alternatively, reference spectra may be obtained by taking raw spectra at different magnetic fields. Since the application of an external magnetic field shifts only the EPR resonance, the division of raw spectra taken at different external magnetic fields results in negative and positive parts in the spectrum. These spectra are referred to as magnetic field division spectra (MDS).[28,29]

Computational Studies. The electronic structures of iron corroles were investigated via quantum chemical theory calculations performed using the ORCA 4[56] and Gaussian 09 software packages.[57] While the investigation of Fe(tpfc)Cl, Fe(tmc)Cl, and Fe(ttc)Ph (see Schemes 1 and S1) used unabridged structural models derived from the experimental crystal structures, that of Fe(tpc)Cl and Fe(tpc)Ph employed geometry-optimized structures. These geometry optimizations were performed using Gaussian 09 on both unabridged and simplified structural models. The latter structures were obtained by replacing the phenyl substituents that decorate the corrole macrocycles with hydrogen atoms (i.e., to give what we refer to as Cor). Density functional theory (DFT) calculations were performed using the B3LYP, BP86, and TPSSh functionals in conjunction with the 6311G basis set.[58−60] Theoretical estimates of the zfs and g matrices were obtained using the coupled-perturbed (CP) DFT formalism and the complete active space (CAS) self-consistent field (SCF) methods as implemented in ORCA 4.2.[61−65] The ground state character of the DFT solutions was confirmed using time-dependent (TD) DFT calculations for which all one-electron excitations were found to be positive. The nature of the predicted electronic configuration, whether it corresponds to a genuine iron(IV) or to an iron(III) coordinated by a noninnocent corrole, was established by inspecting the predicted expectation values of the $\hat{S}^2$ operator, the atomic Mulliken charges, and the Mulliken spin populations. The geometry optimizations, CASSCF, TD, and SCF calculations were terminated upon reaching the default convergence criteria. The CASSCF calculations used simplified structural models obtained from TPSSh/6-311G geometry optimizations. These calculations employed the def2-TZVPP basis set[66,67] and def2/JK auxiliary basis sets in conjunction with the resolution of identity approximation (RI-JK).[68] The quasi-restricted orbitals spanning active space of the initial guess for the CASSCF(4,5) calculations were obtained from single-point DFT (BP and TPPSh) calculations. These orbitals included the canonical 3d orbitals of the iron sites, that is, the nonbonding {xy, xz, yz} and the σ*, {x^2-y^2, z^2}-like molecular orbitals.[69] The converged CASSCF(4,5) results were used as initial guesses for CASSCF(6,6) calculations for which the active space was expanded to include the b_1, HOMO-like of the free corrole. In our case, this ligand-based orbital mixes with the iron $3d_{z^2}$ orbital, yielding a π-like MO straddling the p_z atomic orbitals of tetrapyrrole nitrogen and meso carbon atoms. The active space of the CASSCF(8,7) calculations was derived from that of CASSCF(6,6), which was augmented to include the σ-bonding, $d_{x^2-y^2}$-like orbital. Finally, to evaluate the contributions of excited states to the zfs tensors, we performed CASSCF calculations that included: ten triplet states, 3(10); ten triplets and five quintets, 3(10) 5(5); ten triplets and ten singlets, 3(10) 1(10); and ten triplets, ten singlets, and five quintets, 3(10) 1(10) 5(10).

RESULTS AND DISCUSSION

The results for Mn(tpfc) are relatively straightforward and required only field-domain (HFEPR) techniques and are thus discussed first.

Mn(tpfc). Mn(tpfc) in benzene solution produced excellent-quality HFEPR spectra at any frequency, corresponding to those expected from a high-spin (S = 2) Mn^{III} complex. Manganese(III) thus lived up to its reputation, described as "the deliciae of HFEPR spectroscopists" by the late P. L. W. Tregenna-Piggott.[70] Figure 1 shows one such spectrum, recorded at 326 GHz and accompanied by its simulations,

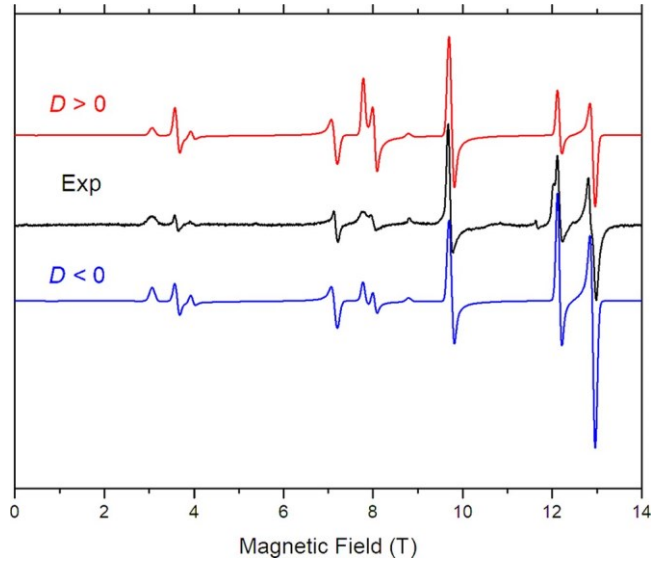

Figure 1. An EPR spectrum of Mn(tpfc) in benzene solution at 30 K and 326.4 GHz (black trace) accompanied by simulations (colored traces) using spin Hamiltonian parameters as in Table 3. Red trace: simulation using a positive D value; blue trace: negative D, which better reproduces the experimental spectrum. (The simulations were normalized to the amplitude of the experimental ~9.7 T turning point.) The doubling of the perpendicular turning point at ~8 T in both experiment and simulations is indicative of a symmetry lower than 4-fold.

one using a positive, and the other a negative D value. By comparing the intensity of particular turning points between experiment and simulations, it becomes obvious that the sign of D in Mn(tpfc) is negative, the significance of which is discussed below. The doubling of the perpendicular turning point at ~8 T is an effect of lowering the symmetry of the zfs tensor from 4-fold as in standard porphyrin to 2-fold in a corrole. Two other spectra recorded at different frequencies and their simulations are shown in the Supporting Information. Despite the high quality of the frozen solution spectra, no ^{55}Mn (I = $^5/_2$, 100%) hyperfine coupling was observed, which is likely a consequence of the spectral line widths originating from field-dependent effects such as D-

DOI: 10.1021/acs.inorgchem.9b02635
Inorg. Chem. 2020, 59, 1075−1090

strain.[71] Hyperfine coupling from $^{55}Mn^{III}$ has been seen in HFEPR only in doped single crystals[70] where the line widths are very narrow.

Figure 2 depicts the 2D field versus frequency plot of the resonances observed for Mn(tpfc). Most, although not all, of the expected transitions were observed so that a tight fit to the spectral data could be obtained. In principle, spectra could have been recorded at relatively low frequencies (<200 GHz), but there was no reason to do this, given instrument time limitations and the successful determination of the spin Hamiltonian parameters from the higher frequency spectra. Moreover, Mn(tpfc) does give EPR spectra at X-band using parallel mode detection: a signal recorded at 5 K yielded g_{obs} = 7.98 with resolved hyperfine splitting ($A(^{55}Mn) \approx 3$ mT).[36] Similar X-band parallel mode EPR spectra have been reported for other $S = 2$ Mn^{III} complexes.[72−75]

Fe(tpc)X, X = Cl, Ph. In addition to our main focus, namely, field- and frequency-dependent magnetic resonance studies, discussed below, we also recorded zero-field

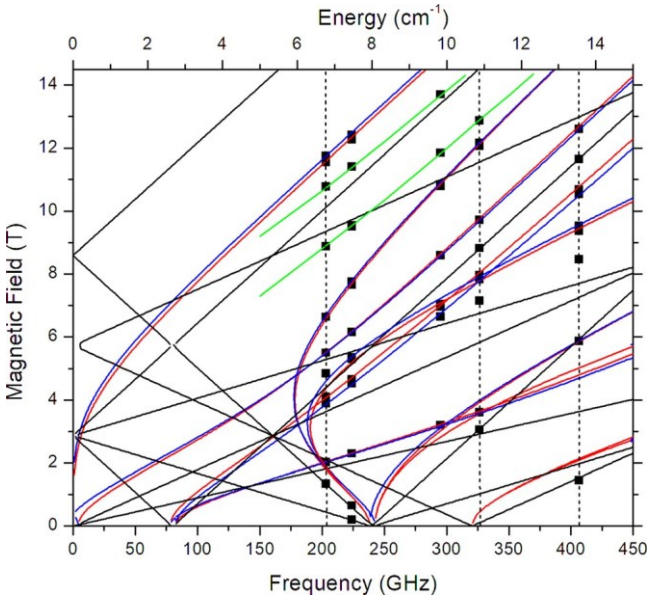

Figure 2. A 2D field vs frequency (or energy) map of turning points in the HFEPR spectra of Mn(tpfc) in benzene solution. The squares are experimental points, while the curves were simulated using spin Hamiltonian parameters as in Table 3. Red curves: turning points with magnetic field oriented parallel to the x-axis of the zfs tensor, blue: $B_0 || y$; black: $B_0 || z$; green: major off-axis turning points. The vertical dashed lines represent the frequencies at which spectra shown in Figures S2, S1, and S3 (Supporting Information), respectively, were recorded.

Mössbauer spectra of the two Fe complexes. Mössbauer spectroscopy has been widely applied to corrole complexes of Fe, as it has been to Fe complexes of every possible type. Specifically, zero-field Mössbauer spectra have been recorded for Fe(dmhec)X,[20,53] Fe(oec)X[52] (X = Cl, Ph), Fe(tpc)Cl,[53] and Fe(tpfc)Cl,[21,76] but to our knowledge, not for Fe(tpc)Ph prior to this study. In addition to providing information on isomer shift (δ) and quadrupole splitting (ΔE_Q) for comparison with literature data, the Mössbauer studies here demonstrate the homogeneity and authenticity of the complexes studied.

The zero-field Mössbauer spectra recorded for Fe(tpc)Cl and Fe(tpc)Ph consist of well-defined quadrupole doublets, see Figure S1 (Supporting Information). The parameters describing the spectra recorded at 130 K and at room temperature along with those of previous work are given in Table 1. Interestingly, the observed resonances are relatively narrow with line widths Γ ~ 0.25 mm/s vs Γ = 0.27−0.35 mm/s for most species, clearly indicating that not only are the two samples investigated analytically pure, but also that these compounds are structurally homogeneous and essentially free of heterogeneous distortions.

The substituents decorating the corrole macrocycle have relatively little effect on the zero-field Mössbauer parameters, suggesting that comparisons between tpc and tpfc complexes are valid. In contrast, altering the apical ligand leads to more substantial changes. For [Fe(tpc)X], replacing a chloride with phenyl leads to not only a larger quadrupole splitting but also to a leftward shift of the entire spectrum (Figure S1). The latter observation demonstrates a lower isomer shift (Δδ ~ −0.28 mm/s), consistent with an increase in oxidation state of the iron site. Although the isomer shift of Fe(tpc)Cl falls between those observed for Fe^{III} (particularly with interTable 1. Zero-Field Mössbauer Parameters of S = 1, (Formally) Fe^{IV} Corrole and Porphyrin Complexes

complex	δ (mm s^{-1})[a]	ΔE_Q (mm s-1)[a]	reference and notes
Fe(tpc)Cl	+0.098(2)[b]	2.889(3)	RT, this work
	+0.170(1)	2.920(2)	130 K, this work
	+0.19	2.93	77 K[53]
Fe(dmhec)Cl	+0.21	3.02	4.2 K[20]
Fe(oec)Cl	+0.21	2.89	4.2 K[20]
	+0.19	2.99	77 K[52]
Fe(tpfc)Cl	0.18	+2.93	80 K[21]
Fe(tpc)Ph	−0.18(1)	3.587(9)	RT, this work
	−0.118(7)	3.641(4)	130 K, this work
Fe(dmhec)Ph	−0.10	3.74	4.2 K[20]
Fe(oec)Ph	−0.10	3.78	4.2 K[20]
	−0.11	3.72	77 K[52]
[Fe(oetpp)Ph]$SbCl_6$	0.13	3.21	4.2 K[77]
[FeO(tdcpp)] CF_3SO_3[c]	0.06	1.48	4.2 K[16]
Fe(tpfc)Br	0.17	3.12	80 K[21]

[a]Signs of δ and ΔE_Q are given where they have been specifically determined/reported. The parameters were determined at either zero field or a small applied field (typically, 20 mT). [b]The error bars were estimated from the combined visual inspection of individual simulations and constrained least-squares fitting of the respective

DOI: 10.1021/acs.inorgchem.9b02635
Inorg. Chem. 2020, 59, 1075−1090

spectra. [c]This species represented 24% of the signal; the major species was an oxidized, Compound I analogue, $[Fe^{IV}O(Por^{\bullet-})]^{+}$.

mediate spin, $S = {}^{3}/_{2}$) and Fe^{IV} ions,[21] that of Fe(tpc)Ph is clearly typical of Fe^{IV} ions. Consequently, the metal site of Fe(tpc)Ph has a stronger +4 character than that of Fe(tpc)Cl for which the iron ion is considered to have an intermediatespin Fe^{III} configuration, as discussed in more detail below.

Fe(tpc)Cl showed strong HFEPR signals above ~300 GHz with a near zero-field resonance observed at 4.5 K and 432 GHz (14.4 cm^{-1}, Figure S4). A spectrum recorded at a higher frequency (624 GHz) is shown in Figure 3 (top) and demonstrates the positive sign of D. A 2-D map of HFEPR resonances (field vs frequency/energy) was compiled and is shown in Figure 4 (top). Subsequently, spin Hamiltonian parameters were best-fit to that map, with the results shown in Table 3. From that map, it became obvious that the near zerofield resonance observed at 432 GHz (Figure S4) represents the D − E transition in the triplet state manifold. The D + E resonance should appear at ~444 GHz, but there was no subTHz source at our disposal to cover that frequency. Instead, the doubling of the perpendicular turning point observed at 624 GHz (Figure 3, top) indicates a finite value of E with the zfs rhombicity factor E/D of about 0.01.

FD-FT THz-EPR spectra of Fe(tpc)Cl are shown in Figure 5 (left), with the absorbance (A) measured in zero field shown in the bottom panel. It is obtained as $A = \log_{10} I_0$ with I_{ref} being a spectrum measured at 30 K and I_0 the spectrum measured at 5 K. The spectrum shows a single absorption line at 14.5 cm^{-1}, which is assigned to the EPR transition between the ground state $|S, m_s\rangle = |1, 0\rangle$ and excited state $|1, \pm1\rangle$. The width of the band gives an estimate as to the rhombic zfs, as two distinct (D + E and D − E) transitions are not observed. With the application of an external field, the Zeeman effect

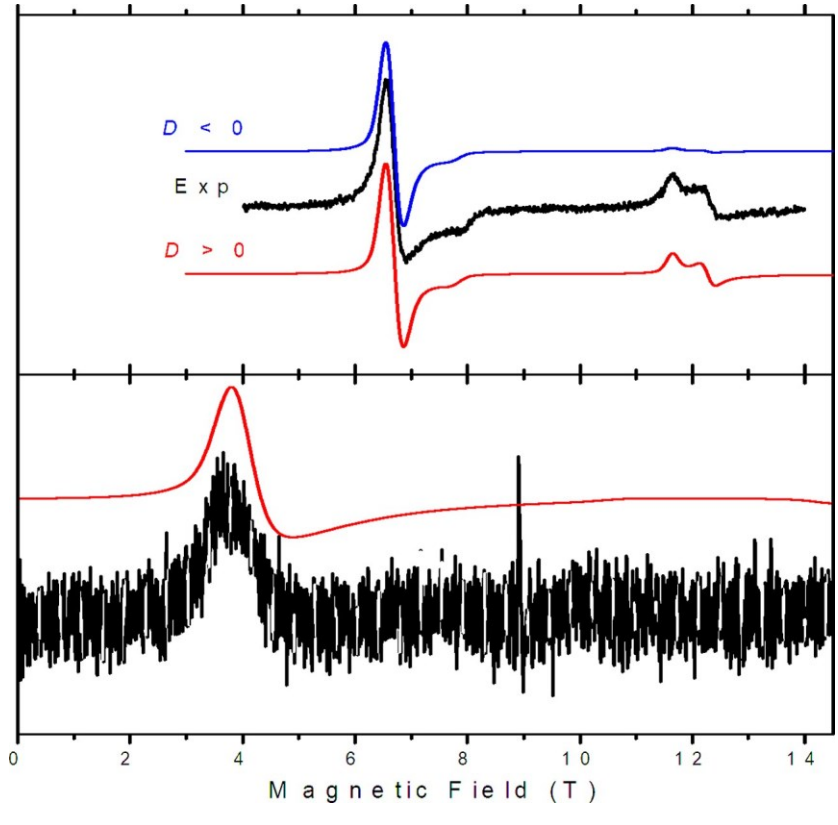

Figure 3. (Top) HFEPR spectrum (black trace) of Fe(tpc)Cl recorded at 4.5 K and 624 GHz accompanied by its simulations (colored traces) using |D| = 14.61 cm^{-1}, |E| = 0.215 cm^{-1}, and g = [2.03, 2.03, 1.95]. Red trace uses D > 0, which reproduces the experiment better than D < 0 (blue trace). (Bottom) HFEPR spectrum of Fe(tpc)Ph recorded at 4.5 K and 514 GHz (black trace) and its simulation (red trace) using |D| = 21.0 cm^{-1}, E = 1.44 cm^{-1}, and g_z = 1.984. The sharp resonance at 8.94 T originates from solid molecular oxygen[78] and is a very convenient field marker.

DOI: 10.1021/acs.inorgchem.9b02635
Inorg. Chem. 2020, 59, 1075−1090

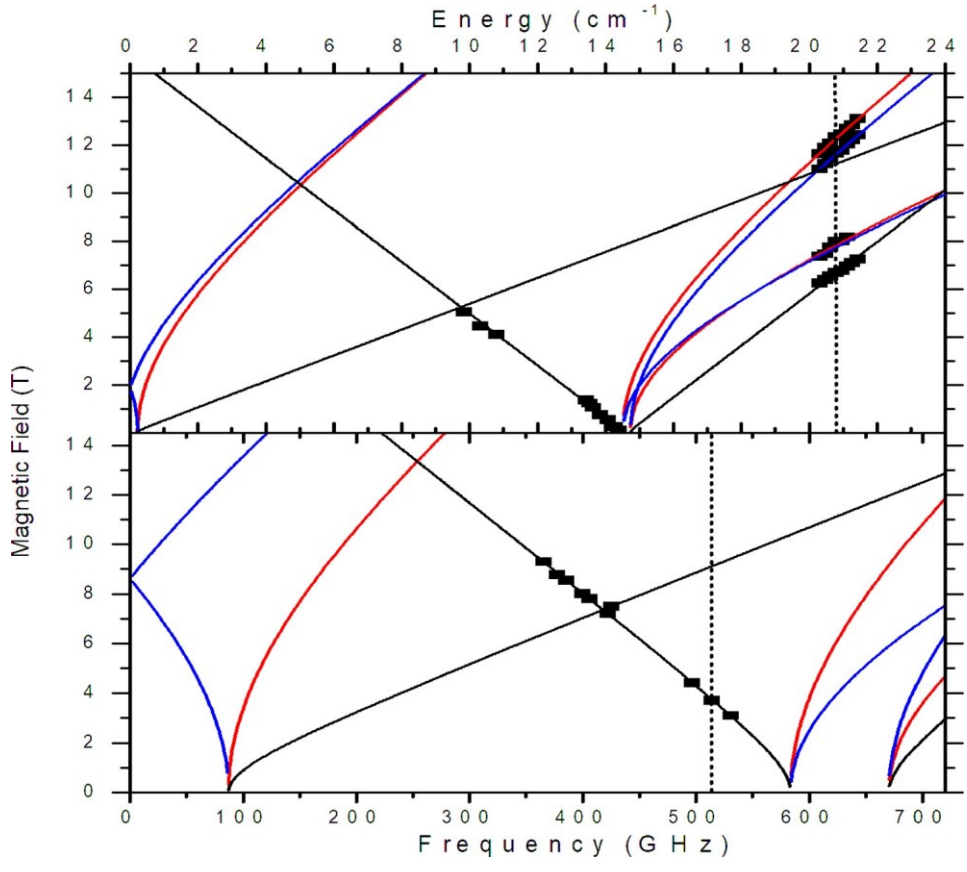

Figure 4. (Top) Map of field vs frequency/energy dependence of the EPR turning points in Fe(tpc)Cl at 4.5 K. The squares are experimental points, while the curves were simulated using best-fit spin Hamiltonian parameters: $|D| = 14.63$ cm^{-1}, $E = 0.159$ cm^{-1}, ($E/D = 0.011$), and g = [2.01, 2.04, 1.99]. Red curves: turning points with magnetic field oriented parallel to the x-axis of the zfs tensor, blue: $B_0 \parallel y$; black: $B_0 \parallel z$. (Bottom) Similar map for Fe(tpc)Ph with simulations using $|D| = 20.9$ cm^{-1}, $E = 1.44$ cm^{-1}, and g = [2.00, 2.00, 1.984]. The vertical dashed lines represent the frequencies at which the spectra shown respectively in Figure 3 (top) and Figure 3 (bottom) were recorded.

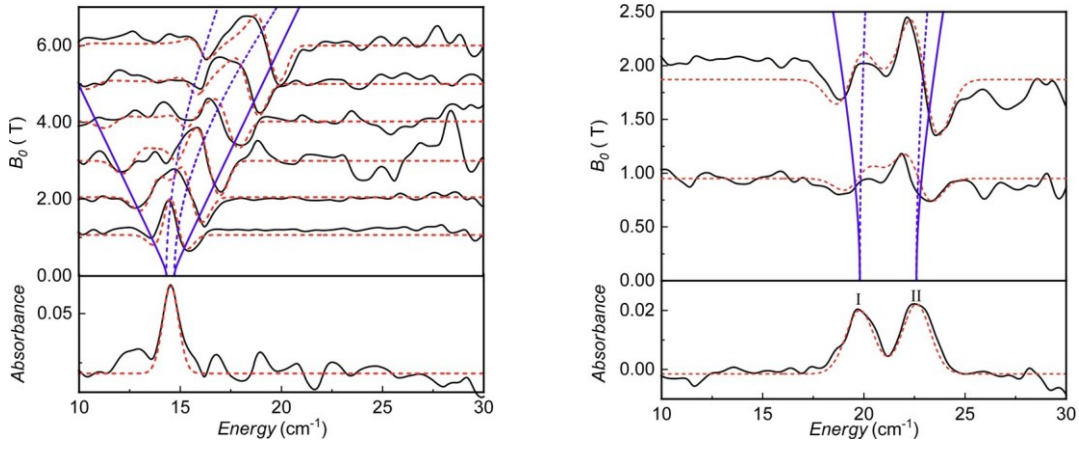

Figure 5. Top panels: FD-FT THz-EPR MDS spectra of Fe(tpc)Cl measured at 5 K (left) and Fe(tpc)Ph measured at 2.5 K (right). Magnetic fields are indicated on the y-axis. Blue lines depict calculated EPR transition energies with respect to the corresponding ground state for $B_0 \parallel z$-axis (solid line) and $B_0 \perp z$-axis (dashed line). Bottom panels: FD-FT THz-EPR absorbance spectra of Fe(tpc)Cl (left) and Fe(tpc)Ph (right) both measured at zero magnetic field. Dashed red lines correspond to simulations with EasySpin[79,80] using $S = 1$, $D = 14.5$ cm^{-1}, $E = 0.2$ cm^{-1}, and g = [2.03, 2.03, 1.95] for Fe(tpc)Cl (left) and $S = 1$, $D = 21.3$ cm^{-1}, $E = 1.0$ cm^{-1}, and g = [2.125, 2.0, 2.0] for Fe(tpc)Ph (right), respectively.

DOI: 10.1021/acs.inorgchem.9b02635
Inorg. Chem. 2020, 59, 1075−1090

causes the transition to split and move with increasing field. This behavior is modeled using the following parameter sets: D = 14.5 cm^{-1}, E = 0.2 cm^{-1}, and g = [2.03, 2.03, 1.95].

The field dependent behavior of the magnetic resonance signals is more easily seen using an energy level diagram, as shown in Figure 6. The lines were calculated using the same set of spin Hamiltonian parameters as in Figure 5.

The exact same sample of Fe(tpc)Ph used for FD-FT THzEPR was subsequently used for HFEPR. The HFEPR response was about an order of magnitude weaker than that of Fe(tpc) Cl measured under identical conditions including the same

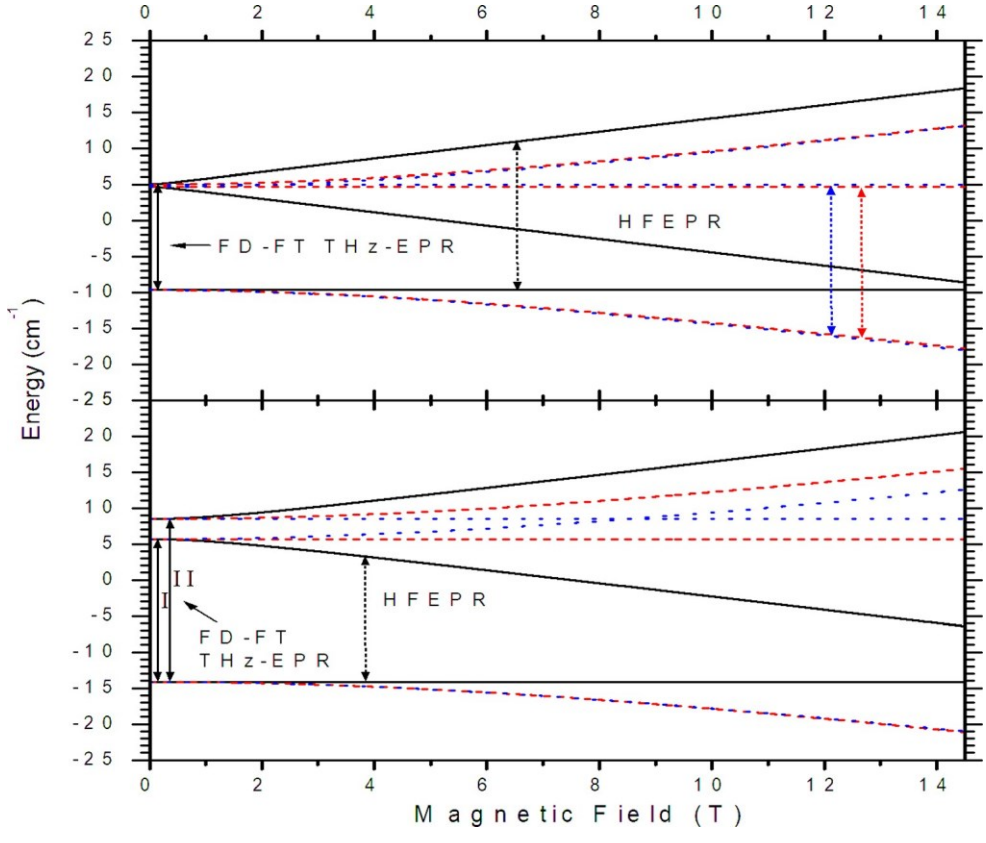

Figure 6. (Top) Calculated magnetic field dependence of the spin state energies of Fe(tpc)Cl for B_0 || z-axis (solid black line) and $B_0 \perp$ z-axis (overlaid dashed red (B_0 || x) and blue (B_0 || y) lines) with S = 1, D = 14.53 cm^{-1}, E = 0.2 cm^{-1}, and g = [2.03, 2.03, 1.95]. (Bottom) Similar plot for Fe(tpc)Ph with S = 1, D = 21.2 cm^{-1}, E = 1.4 cm^{-1}, and g = [2.125, 2.00, 2.00]. In this case, the rhombic zfs is sufficient that the lines corresponding to B_0 || x (red) and B_0 || y (blue) can be distinguished for the higher energy spin manifold, but not in the lower one, in which case overlaid dashed lines are used.

Table 2. Spin Hamiltonian Parameters for S = 2 Mn^{III} Corrole and Porphyrin Complexes

complex	D (cm^{-1})[a]	|E| (cm^{-1}), |E/D|	g[b]	references and notes
Mn(tpfc)	−2.67(1)	0.023(5), 0.009	1.992(3), 2.006(3), 2.002(6)	HFEPR, benzene frozen solution, this work
Mn(dehmc)[c]	−2.64(1)	0.015(5), 0.0057	2.02(1), 2.00(1)	HFEPR, immobilized powder[48]
Mn(dehmc)(py)	−2.78(1)	0.030(5), 0.011	2.00(2), 2.00(2)	HFEPR, Mn(dehmc) in pyridine frozen solution[48]
Mn(tpfc)($OPPh_3$)	−2.69(2)	0.030(3), 0.011	1.994(4), 1.980(4)	HFEPR, powdered solid[47]
Mn(tpp)Cl[d]	−2.290(5)	0.00(1), 0	2.005(3), 1.98(2)	HFEPR, immobilized powder[83]
Mn(oep)Cl[e]	−2.40(1)	0.02(1), 0	2.00(1)	HFEPR, in toluene/dichloro-methane (2:3) frozen solution[38]
Mn(oep)Br[e]	−1.07(1)	0.00(3), 0	2.01(1), 1.98(1)	HFEPR, powdered solid[38]
Mn(tpp)(Me_2pyNO)$_2$[f]	−3.817(4)	0.160(4), 0.042	2.013(5), 2.001(4), 1.994(4)	HFEPR, immobilized powder[41]
Mn(Nctpp)(py)$_2$[g]	−3.084(3)	0.608(3), 0.197	2.000(2), 2.000(3), 2.006(4)	HFEPR, powdered solid[96]
Mn(tsp)[h]	−3.16(2)	0.00(1), 0	2.00(2)	HFEPR, frozen aqueous solution[40]
MnMb[i]	−3.79(3)	0.08(1), 0.02	2.0	HFEPR, frozen aqueous solution[43]

DOI: 10.1021/acs.inorgchem.9b02635
Inorg. Chem. 2020, 59, 1075−1090

[a]The error bars for all spin Hamiltonian parameters obtained by HFEPR in this work (row 1) are standard deviations in the least-squares fits to the 2D field/frequency maps such as the one shown in Figure 2. [b]In the case where all three g matrix components were determined, these are given in order g_x, g_y, g_z (or g_{min}, g_{mid}, g_{max}); if two values are quoted, they are shown as $g_\perp$ and $g_{||}$, and if only one value is given, then only an isotropic g value was determined. [c]dehmc is 8,12-diethyl-2,3,7,13,17,18-hexamethylcorrole trianion. [d]tpp is 5,10,15,20-tetraphenylporphyrin dianion. [e]oep is 2,3,7,8,12,13,17,18-octaethylporphryin dianion. The |E| value reported for Mn(oep)Cl in frozen solution is an upper limit based on line widths.[38] [f]
Me_2pyNO is 3,5-dimethylpyridine N-oxide, which is bisaxially coordinated. The HFEPR spectral simulations also yielded a fourth order zfs term, $B_4^4 = 20(5) \times 10^{-4}$ cm^{-1}.[41] [g]Nctpp is 5,10,15,20-tetraphenyl-N-confused porphyrin trianion (i.e., a pyrrole has been inverted so that it is exo to the macrocycle, 2-aza-21-carbaporphyrin). The complex has biaxial pyridine ligands. [h]tsp is 5,10,15,20-tetra(4-sulfonatophenyl)porphyrin dianion.[97] The solid complex is obtained as the acid form chloride, Mn(tsp)Cl, but the sulfonate groups are presumably deprotonated, and the chlorido ligand is aquated, to give primarily $[Mn^{III}(tsp^{6-})(H_2O)_2]^{3-}$ in neutral aqueous solution by analogy with reported studies on Mn(tsp) and related Mn^{III} complexes of porphyrins with anionic and cationic substituents.[98] [i]Mb is myoglobin; in this case, manganese(III) protoporphyrin IX reconstituted myoglobin, which has an axial aqua ligand and the proximal histidine (imidazole) ligand.[99]

sample mass. Nevertheless, an agreement with the frequency- value for one g matrix component (g_z) could be accurately domain results (see below) obtained within 1.5% for |D| plus a determined.

DOI: 10.1021/acs.inorgchem.9b02635
Inorg. Chem. 2020, 59, 1075−1090

Table 3. Spin Hamiltonian Parameters for S = 1 (Formally) Fe^{IV} Corrole, Porphyrin, And Related Complexes

complex	D (cm^{-1})[g]	|E| (cm^{-1}), |E/D|	$g_{\perp}$, $g_{\parallel}$[h]	References and notes
Fe(tpc)Cl this work	[redacted]			
	+14.5(2)	<0.2, 0.01	2.03(5), 1.95(5)	FD-FT THz-EPR, this work
Fe(dmhec)Cl	28	0	2.0, 2.0	magnetic susceptibility[20]
Fe(tpfc)Cl	14.1	1.0, 0.07	2.0	applied-field Mössbauer[21]
Fe(tpc)Ph	+20.9(1)	1.44(5), 0.069	2.00, 1.984(5)	HFEPR, this work
	+21.3(2)	1.0(2), 0.05	2.1(1), 2.0 (1), 2.0(1)	FD-FT THz-EPR, this work
Fe(dmhec)Ph	20	0	2.06, 2.00	magnetic susceptibility[20]
$[Fe(oetpp)Ph]SbCl_6$	30.5	0	2.20, 1.98	Mössbauer, solid[77]
$[FeO(tdcpp)]CF_3SO_3$	25	1.9, 0.075	2.2, 2.24, 1.99	Mössbauer, vacuum-dried solid, subspecies (24%), with major species a Compound I analogue
$[Fe(O)(tmc)(MeCN)]^{a}(CF_3SO_3)_2$	+26.95(5)	0.070(35), 0.002	2.10(5), 2.04(1)	HFEPR, powdered solid[108]
$[Fe(O)(tmc)(CF_3CO_2)]^{b}(CF_3CO_2)$	31(2)	0		Mössbauer, solid[116]
$[Fe(O)(tmcs)]^{+c}$	35(3)	0		Mössbauer, frozen MeOH solution[117]
$[Fe(O)(tmc\text{-}py)]^{2+d}$	29(2)	0.15, 0.005		Mössbauer, frozen MeCN solution[118]
$[Fe(O)(cyclam\text{-}CH_2CO_2)]^{+e}$	23(2)	0	2.0	Mössbauer, frozen acetone/water solution[119]
$[Fe(O)B^*]^{2-f}$	24(3)	0		Mössbauer, frozen aqueous solution[120]

[a] tmc is 1,4,8,11-tetramethyl-1,4,8,11-tetraazacyclotetradecane. It should be noted that a stereoisomer of this complex (studied in frozen MeCN solution by Mössbauer) in which the macrocycle is "inverted" gave the same zfs parameters as the crystallographically characterized stereoisomer studied by HFEPR. The "inverted" complex, however, showed enhanced reactivity in HAT and OAT processes.[121] [b]This is but one of an extensive series of complexes of general formula $[Fe(O)(tmc)X]^+$, where X = $CF_3CO_2^-$ (31), NCO^- (31), NCS^- (30), N_3^- (29), CN^- (31), HO^- (31), studied by Mössbauer in frozen MeCN solution (except for X = $CF_3CO_2^-$, which is a stable solid) to yield D values, which are given here in parentheses (in cm^{-1}).[116] The uncertainty in D for all of these was 2 cm^{-1}; there was no need to introduce any rhombic zfs, so E ≈ 0. [c]tmcs is 2(4,8,11-trimethyl-1,4,8,11-tetraaza-cyclotetradec-1-yl)-ethanethiol monoanion. The ferryl unit thus has an axial thiolato ligand directly connected to the macrocycle. [d]tmc-py is 1-(2-pyridylmethyl)-4,8,11-trimethyl-1,4,8,11-tetraazacyclotetradecane. The ferryl unit thus has an axial pyridine ligand directly connected to the macrocycle. The E/D value of 0.15 is taken directly from Table S1 of Thibon et al.,[118] but seems remarkably large in light of the $[Fe(O)(tmc)X]^{2+,+}$ results.[116] [e]cyclam-CH_2CO_2 is 1,4,8,11-tetraazacyclotetradecane-1-acetate monoanion. The ferryl unit thus has an axial acetato ligand directly connected to the macrocycle. The E value was fixed to 0, and g was fixed at 2.0.[119] [f]B* is 7,7,10,10,13,13-hexamethyl5,7,8,12,13,15-hexahydro-5,8,12,15-tetraazabenzocyclotridecene-6,9,11,14-tetraone tetraanion. The ferryl unit thus has four amidate nitrogen equatorial donors and no axial ligand. [g]Signs of D are given where they have been specifically determined/reported. The error bars for all spin Hamiltonian parameters obtained by HFEPR in this work are standard deviations in the least-squares fits to the 2D field/frequency maps such as the one shown in Figure 4. If no error bar is given, then the parameter was fixed in the fits. [h]In the case of HFEPR, the g values were experimentally determined, in some cases for all three components; in the case of Mössbauer studies, g values of 2 were assumed. [i]The accuracy of zfs values obtained by FD-FT THz-EPR is 0.2 cm^{-1} for a FTIR resolution of 0.5 cm^{-1}. This accuracy can be reached by simultaneous simulation of FD-FT THz-EPR MDS and absorbance spectra with one set of spin Hamiltonian parameters. [j]This D value for Fe(dmhec)Cl was determined for the Fe^{III} component of an antiferromagnetic exchange coupled two spin system (S_{Cor} = $^1/_2$; S_{Fe} = $^3/_2$) with total S = 1[20] and is thus not directly comparable to the D value for the total S = 1 system, as was the case for Fe(tpfc)Cl.[21] Spin-coupling coefficients[23] indicate that for $|D_{Fe}|$ = 28 cm^{-1}, $|D_{S=1}|$ = 42 cm^{-1}; to obtain $D_{S=1}$ = 14 cm^{-1}, $|D_{Fe}|$ = 9.35 cm^{-1} is required.

Figure 3 (bottom) shows the EPR spectrum of Fe(tpc)Ph recorded at 514 GHz and 4.5 K. The broad resonance at ~3.9 T is a parallel turning point of the triplet powder spectrum (the perpendicular turning points situated outside the magnet range). The resonance could be followed only in a relatively narrow frequency range, from 360 to 530 GHz. In particular, it was not possible to detect the resonance near its zero-field transition frequency (~600 GHz) as the available power was not sufficient. The 2D field versus frequency map of the sole observed turning point is shown in Figure 4 (bottom).

Frequency-domain EPR spectra of Fe(tpc)Ph are shown in Figure 5 (right), with I_{ref} being a spectrum measured at 35 K and I_0 the spectrum measured at 2 K. In contrast to the results for Fe(tpc)Cl, the zero-field spectrum (bottom panel) shows two absorption lines at 19.76 cm^{-1} (line I) and 22.57 cm^{-1} (line II). The splitting gives an accurate measure as to the

DOI: 10.1021/acs.inorgchem.9b02635
Inorg. Chem. 2020, 59, 1075−1090

rhombic zfs parameter (E), as two distinct (D + E and D − E) transitions are observed. With the application of an external field, the Zeeman effect causes the transitions to split further and move with increasing field. This behavior is modeled using the following parameter set: D = 21.2 cm^{-1}, E = 1.0 cm^{-1}, and g = [2.125, 2.0, 2.0].

The spin Hamiltonian parameters obtained from field- and frequency-domain magnetic resonance studies for Mn(tpfc) and the two Fe corrole complexes, Fe(tpc)Cl and Fe(tpc)Ph, are summarized in Tables 2 and 3 for each metal ion, respectively. Also included in each table for comparison are literature values for related complexes. In the case of Mn(tpfc), these include the two Mn^{III} corrole complexes studied previously by HFEPR[47,48] and representative Mn^{III} porphyrin complexes. A recent, extensive tabulation of spin Hamiltonian parameters in Mn^{III} complexes is given by Tadyszak et al.[42] The zfs of high-spin $3d^4$ ions (e.g., Cr^{II} and Mn^{III}) in tetragonally distorted octahedral geometries (including both square pyramidal−one axial ligand at infinite distance, and square planar−both axial ligands at infinite distances) is relatively well described by simple ligand-field theory (LFT), and has been discussed at length elsewhere.[42,72,81−85] In-depth computational studies of zfs in Mn^{III} species have also been reported.[63,86,87] Briefly, a negative axial zfs, D < 0, corresponds to a tetragonal elongation ("hole" in the $d_{x^2-y^2}$ orbital; $^5B_1$ ground state), while a positive axial zfs, D > 0, corresponds to a compression, which also corresponds to the situation for trigonal bipyramidal geometry ("hole" in the d_{z^2} orbital; $^5A_1$ ground state).[88,89] The former situation applies to most 6coordinate,[90−92] 5-coordinate (square pyramidal), and 4-coordinate (square planar) Mn^{III} complexes.[93−95,38]

As seen in Table 2, the zfs parameters of the Mn^{III} ion in a square planar corrole are essentially the same whether the corrole ligand has relatively electron donating alkyl (methyl and ethyl) substituents as in the case of Mn(dehmc) or relatively electron withdrawing pentafluorophenyl substituents as in Mn(tpfc). Also notable is that the effect of a single axial ligand, as least when it is $OPPh_3$, is negligible based on the comparison between Mn(tpfc) and Mn(tpfc)($OPPh_3$). Even the Mn^{III} porphyrin complexes, when in square pyramidal geometry, exhibit zfs parameters very close (within ∼15%) to those for the corroles, although such species are axially symmetric, as expected from the 4-fold symmetry of the porphyrins listed. When the tetrapyrrole complex is 6coordinate, the zfs approaches the larger magnitude seen in 6-coordinate complexes such as $Mn(acac)_3$ (acac = 2,4pentanedione monoanion), for which D = −4.52 cm^{-1}.[72] Although deeper insights can be gained by use of sophisticated quantum chemical theory analysis,[86] the zfs of Mn^{III} in corrole and porphyrin is relatively unambiguous. Should a formally Mn^{III} corrole, porphyrin, or other such tetrapyrrole complex with only light atom (n = 2, 3) ligands exhibit zfs deviating significantly from the representative situations given in Table 2, (e.g., D ≈− 2.5 ± 0.5 cm^{-1} for 4- or 5-coordinate; D ≈− 3.5 ± 0.5 cm^{-1} for 6-coordinate), then its conventional description as $[Mn^{III}(Cor^{3-})]^0$ or $[Mn^{III}(P^{2-})]^+$ (Cor = corrole, P = porphyrin) is likely suspect.

The above "rule of thumb" for Mn^{III} corrole and porphyrin complexes can be contrasted with the results obtained here for the two formally Fe^{IV} corrole complexes, Fe(tpc)X, X = Cl, Ph. In contrast to the many Mn^{III} examples (see Table 2), no Fe^{IV} tetrapyrroles had been studied by HFEPR prior to this work. However, applied-field Mössbauer has been widely applied to a variety of tetrapyrrole complexes of Fe^{IV}, including a corrole, Fe(tpfc)Cl (see Table 3).[21] Applied-field Mössbauer has provided spin Hamiltonian parameters for porphyrins as well, such as [Fe(oetpp)Ph]$SbCl_6$ (oettpp = 2,3,7,8,12,13,17,18octaethyl-5,10,15,20-tetraphenylporphyrin dianion) which, like Fe(tpc)Ph, is a bona fide Fe^{IV} complex and not a coupled radical.[77] Most Mössbauer (and conventional EPR) studies on porphyrins, however, have been on Compound I species[12−16] which, by virtue of being formally Fe^{V}, are not germane to this study. We note that in the study of the Compound I analog, $[FeO(tdcpp)]^+$ (tdcpp = 5,10,15,20-tetrakis(2,6dichlorophenyl)porphyrin dianion), the reduced (Compound II) species, [FeO(tdcpp)], was observed as an undesired, minor component (24%), and its parameters are given in Table 3.[16]

A difficulty with respect to field- and frequency-domain EPR studies of Fe^{IV} tetrapyrroles is that $[Fe^{IV}(P^{2-})]^{2+}$ species are unstable in comparison to the "thermodynamic sink" of, e.g., Mn(tpp)Cl. However, landmark work by Groves et al. in 1985 brought forth the stable complex Fe(tmp)$(OMe)_2$ (tmp = 5,10,15,20-tetramesitylporphyrin dianion).[100] Its Mössbauer characterization was insufficient (maximum applied field of 40 mT) to allow spin Hamiltonian parameters to be extracted, but the complex clearly had an S = 1 spin ground state.[100] Much more recently, Groves and coworkers showed that watersoluble versions of H_2tmp, namely H_2tsmp (5,10,15,20tetra(3,5-bis-sulfonatomesityl)porphine) and H_2tmps (5,10,15,20-tetra(3-sulfonatomesityl)porphine), could be used to prepare oxidoiron(IV) ($[Fe^{IV}O]^{2+}$, ferryl) complexes Fe(O)(tsmp) and Fe(O)(tmps), which were then used for oxygen atom transfer (OAT) reactivity studies.[101] The investigation by HFEPR (including frequency-domain techniques) and (high) applied-field Mössbauer spectroscopies would be very desirable to help elucidate the electronic structure of these complexes. However, the zfs of formally Fe^{IV} corrole has been determined by applied-field Mössbauer in one case: Fe(tpfc)Cl (see Table 3).[21]

For further comparison, Que and coworkers have reported a large number of $[Fe^{IV}O]^{2+}$ complexes with a wide variety of ligands.[102−107] In most cases, these complexes were

DOI: 10.1021/acs.inorgchem.9b02635
Inorg. Chem. 2020, 59, 1075−1090

analyzed by applied-field Mössbauer and in some cases also by HFEPR,[108–110] so that spin Hamiltonian parameters were definitively determined. Of relevance here are the complexes that, like the tetrapyrroles, exhibit approximate tetragonal symmetry (four equatorial ligands), and these generally have S = 1 spin ground states, as do Fe(tpc)X. In contrast, $[Fe^{IV}O]^{2+}$ complexes in approximate trigonal symmetry (three equatorial ligands) have S = 2 spin ground states, which is what is also found in nonheme iron enzyme intermediates.[107,111] The relevance of the two spin states to model compound and enzyme activity is a topic of intense interest[112,113] but is beyond the scope of the present magnetic resonance study. A comprehensive listing of $[Fe^{IV}O]^{2+}$ complexes including D values is given by McDonald and Que.[106] We thus list only those $[Fe^{IV}O]^{2+}$ species most akin to the corrole complexes studied herein, namely those with macrocyclic ligands. Among these, by far the majority are of the venerable tmc (1,4,8,11tetramethyl-1,4,8,11-tetraazacyclotetradecane)[114] (see Scheme S2) and related macrocycles.[115] However, the D values, as determined by Mössbauer or in one case by HFEPR,[108] for $[Fe^{IV}O]^{2+}$ complexes bearing linear, multidentate (usually pentadentate) ligands have little difference from those given in Table 3, their range being $22 \leq D < 30$ cm^{-1}.

As can be seen from Table 3, $[Fe(O)(tmcs)]^{+}$ (2-(4,8,11trimethyl-1,4,8,11-tetraaza-cyclotetradec-1-yl)-ethanethiol monoanion) has a D value that is at the upper end of those available.[106] It differs from the others of this type solely by virtue of the axial sulfur donor. As noted by Bukowski et al.,[117] this complex is the most analogous to Compound II in heme oxidases, in which the ferryl heme is axially coordinated by cysteine thiolate.[122] Otherwise, the nature of the axial (i.e., trans to oxido) ligand has little effect on the D value of $[Fe^{IV}O]^{2+}$ species, as seen in particular for the $[Fe(O)(tmc)X]^{2+/1+}$ series.[116] Even the complex $[Fe(O)B^{*}]^{2-}$ has a zfs similar to that of the $[Fe(O)(tmc)X]^{2+/1+}$ series. This correspondence is remarkable given that the former complex contains the tetraamidate macrocycle (TAML) developed by Collins,[123,124] with its 4− charge and is lacking an axial ligand, while the latter complex has a neutral tetraamine macrocycle that has no ability to be noninnocent and has various axial ligands.[125] It is then safe to assert that, if one is willing to describe the ferryl ion as comprising Fe^{IV}, then the zfs of bona fide Fe^{IV} should be $D \approx +27 \pm 5$ cm^{-1}. This absolute error bar is moderately large, but the relative value is ~20%, which is the same as the relative value for Mn^{III} tetrapyrroles. Where then, using this simple criterion, do the two formally Fe^{IV} corrole complexes studied here fit in? Fe(tpc)Ph has $D \approx 21$ cm^{-1},[126] which is on the lower end of this range but is still reasonable as a complex of Fe^{IV}. Qualitatively, this lower D value may reflect the higher covalency of the unsaturated π-interacting corrole macrocycle relative to saturated tetraaza macrocycles, disregarding the effect of axial ligand(s). In contrast, Fe(tpc)Cl has $D \approx 14.6$ cm^{-1}, and Fe(tpfc)Cl likewise has $D \approx 14.1$ cm^{-1}, reliably determined by applied-field Mössbauer.[21] This $D < 15$ cm^{-1} is far below that of any Fe^{IV} species and would thus seem not at all to be bona fide Fe^{IV}. Both of these zfsbased assignments are in agreement with the study by Ganguly et al., which employed optical spectroscopy, electrochemistry, and most importantly, X-ray absorption spectroscopy (XAS; specifically K-edge X-ray absorption near-edge spectroscopy, XANES) to probe the nature of Fe(tpc)Cl, Fe(tpc)Ph, and related complexes.[10] The 1s → 3d transition probed by XANES is perhaps the best measure of oxidation state in transition metal complexes, and Ganguly et al. clearly showed that Fe(tpc)Ph is consistent with an Fe^{IV} description (i.e., $[Fe^{IV}(tpc^{3-})]^{+}$), while Fe(tpc)Cl is consistent with an Fe^{III} description (i.e., $[Fe^{III}(tpc^{\bullet 2-})]^{+}$). The contrast between these two types of iron corrole is shown quantitatively in the results of DFT calculations in Figure S6.

Qualitatively, it appears that just as the thiolato ligand in $[Fe(O)(tmcs)]^{+}$ led to an anomalous D value (~30% higher than the above proposed "typical" value), the chlorido ligand leads to a truly anomalous D value—half that seen in typical $[Fe^{IV}O]^{2+}$ complexes and 30% lower than that for the

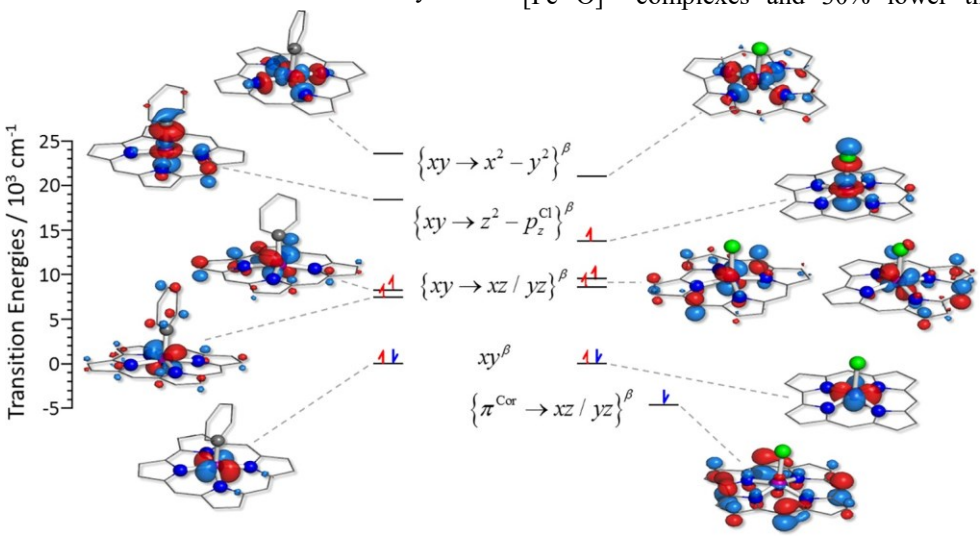

Figure 7. TD-DFT-derived crystal field splitting diagram predicted for Fe(tpc)Ph (left) and Fe(tpc)Cl (right). These plots were obtained for the simplified, geometry-optimized structures. Both the TD DFT and geometry optimizations were performed at the TPSSh/6-311G level of theory. The surface plots were obtained using an isosurface value of 0.04 e/Bohr.[3] The zero energy level corresponds to the S = 1 ground state for each complex.

DOI: 10.1021/acs.inorgchem.9b02635
Inorg. Chem. 2020, 59, 1075−1090

arylcoordinated iron corrole. We suspect that Fe(tpfc)Br[21] would show even more anomalous zfs and add this complex to the "wish list" of tetrapyrroles to be studied by field- and frequency-domain EPR. A quantitative understanding of the effect of axial ligand in metallocorroles to "tempt" the corrole from "innocence" to "noninnocence" is beyond the scope of this study, as is the origin of the lower magnitude D value in such species,[127,128] but it is clear that the zfs in formally Fe^{IV} corroles can be diagnostic as to the true nature of the complex. To gain a deeper understanding of the observed spectroscopic parameters, we used CP-DFT and preliminary CASSCF calculations to derive theoretical estimates of iron corrole zfs values and g matrix components (see Tables S1, S2, and S5, Supporting Information). CASSCF has been previously applied to Fe(tpc)Cl to confirm its noninnocent description, but its spin Hamiltonian parameters had not been investigated, as such information was then unavailable.[22] The results obtained here for simplified and geometry optimized structures mirror closely those obtained for experimental structures. This observation implies that, as expected, the meso-carbon substituents decorating the corrole rings have little sway on the electronic structure of the iron site. Consistent with previous reports,[7,22] we find that the predicted oxidation of the iron sites is essentially determined by the apical ligand, changing from a genuine Fe^{IV} for Fe(tpc)Ph to an Fe^{III} coordinated by a radical for Fe(tpc)Cl (see Figure S6 and Table S4, Supporting Information). This trend is reproduced not only by our DFT calculations but also by CASSCF (see Table S6, Supporting Information). The CASSCF-predicted ground state of Fe(tpc)Ph is dominated by a single determinant, while that of Fe(tpc)Cl originates from the linear combination of several configurations that have a different number of electrons on the metal site and on the ligand (see Table S9, Supporting Information).

The TD-DFT-derived crystal-field splitting diagram of Fe(Cor)L is shown in Figure 7. This orbital splitting is very similar to that inferred for oxidoiron(IV) complexes supported by macrocyclic ligands, in particular that of $[FeO(tmc)(MeCN)]^{2+}$ and $[FeO(tmcs)]^{+}$.[117] The lowest iron 3d orbital, xy, is doubly occupied and essentially nonbonding. However, unlike oxidoiron(IV) moieties for which the singly occupied orbitals of the {xz/yz} quasi-doublet are involved in strong π covalent interactions with the oxido ligand, in both of our cases, the {xz/yz} are not as mixed with axial ligand orbitals, and thus are largely nonbonding.

Interestingly, the redox noninnocent behavior of the corrole ligand is mediated by the symmetry-allowed interaction of the $3d_{z^2}$ metal orbital with the corrole's HOMO. However, in the case of Fe(tpc)Ph, the mixing of these two orbitals is hampered by the very strong σ-type interaction of $3d_{z^2}$ with the ipso carbon atom (see Figure S7, Supporting Information). The second-order perturbation theory expressions derived using the orbital splitting diagram of Figure 7, equations S1 and S2, suggest that the smaller D value of Fe(tpc)Cl is due to the population of the $3d_{z^2}$ orbital. Thus, the intermediate-spin iron(III) site lacks excited states originating from $\{xy/yz \rightarrow z^2\}^{\beta}$ excitations. While the CP-DFT-predicted SOMO → VMO (α→α) contributions to zfs listed in Table S3 seem to corroborate this conclusion, the SOMO → SOMO (α → β) excitations also contribute significantly to the difference between these two zfs values. The latter contributions originate from the spin−orbit coupling of the ground state with excited singlet states and seem to be almost as large as those of the excited triplet states. This situation is in stark contrast to that of the $[FeO(tmc)(MeCN)]^{2+}$ and $[FeO(tmcs)]^{+}$ oxidoiron(IV) complexes for which the largest contribution to their zfs originates from the spin−orbit coupling of a low-lying quintet excited state into the ground state.[117]

Among the three functionals considered (B3LYP, BP86, and TPSSh), only TPSSh reproduced the correct magnitude of the experimental D values. Thus, B3LYP and BP86 predicted D ≈ 3 cm^{-1} for both Fe(tpc)Cl and Fe(tpc)Ph. In contrast, TPSSh predicted D = +16.28 cm^{-1} for Fe(tpc)Cl and +17.61 cm^{-1} for Fe(tpc)Ph for their respective simplified, geometry-optimized structures. The relative performance of these three functionals is markedly different in this case than for Mn^{III} complexes, for which BP86 and B3LYP performed significantly better than TPSSh.[86,129] Our CASSCF calculations done for Fe(tpc)Ph on the TPSSh optimized structure reproduce the salient features of the DFT calculations. Thus, the spin−orbit mixing of excited singlet states with the triplet ground state accounts for nearly 40% of the predicted D value. However, when quintet states were included CASSCF often failed to predict the correct ground spin state, yielding a quintet instead of a triplet ground state. Perhaps this observation is not surprising considering that Hartree−Fock overstabilizes high-spin configurations.[130] For Fe(tpc)Ph the best agreement between the experimental and theoretical D value, +20.9 versus +19.0 cm^{-1}, was obtained when singlet states were included and an extended active space, CASSCF(8,7), was considered (see Tables S5−S10, Supporting Information). Unlike for Fe(tpc)Ph, CASSCF performs considerably worse for Fe(tpc)Cl yielding, e.g., for CASSCF(6,6), a theoretical value, D = 8.77 cm^{-1}, that is only 60% of the experimental value, D = 14.63 cm^{-1}. However, these calculations clearly demonstrate that the ground state of Fe(tpc)Cl cannot be described using a single Slater determinant and that including the HOMO of the corrole ligand plays a crucial role in the magnetic properties of this compound. These calculations also show qualitatively that the zfs for such a noninnocent system is lower magnitude than that for bona fide Fe^{IV}.

A final comment is warranted on the g values to contrast with the zfs. Although magnetic susceptibility and applied-field Mössbauer spectroscopy (for Fe complexes) can provide g values, these are best obtained using EPR. In

DOI: 10.1021/acs.inorgchem.9b02635
Inorg. Chem. 2020, 59, 1075−1090

transition metal ion $S = {}^1/_2$ complexes, the g matrix contains critical information,[55,82,131] especially for systems with large SOC interactions such as in low-spin d^5 which leads to large g anisotropy.[132] In our experience on HFEPR of $S > {}^1/_2$ transition metal systems, however, the g values are relatively uninformative in that they are typically relatively isotropic, although they can be greater than g_e in the case of, e.g., $S = {}^3/_2$ Co^{II} or $S = 1$ Ni^{II}.[24,26,27] But in other cases, particularly for $S = 2$ Mn^{III} complexes, the g values are isotropic and very close to g_e, as can been seen in Table 2 and elsewhere.[42] We have also found by HFEPR[108] that the g values for ferryl complexes are relatively close to g_e. This result is in conflict with LFT,[133] which suggests large deviations from g_e in $S = 1$ d^4 systems.[134] In contrast, the LFT model of Oosterhius and Lang[133] explains reasonably well the large magnitude, positive D values of (bona fide) Fe^{IV} complexes, so that LFT is appropriate to use in such systems. A question arose in the study of $[Fe(O)(tmc)X]^{+,2+}$:[108] what about the g values in tetrapyrroles? We now see that even in the case of Fe(tpc)Ph, the g values are relatively close to g_e. This is also true for Fe(tpc)Cl, but that finding might qualitatively be ascribed to its $[Fe^{III}(tpc^{\bullet 2-})]^+$ description. The CP-DFT calculations done here are consistent with this result in that the predicted average g value is $g_{avg} \approx 2.04(1)$, regardless of whether the experimental or optimized geometries are used or even whether the axial ligand is Cl or Ph (see Tables S1 and S2). Ab initio calculations were not used for the g values, only the zfs, but given the experimental values, this effort did not seem worthwhile. Overall, the zfs is the key spin Hamiltonian parameter in $S > {}^1/_2$ transition metal systems in terms of providing information on electronic structure.

CONCLUSIONS

The Mn^{III} ($3d^4$) corrole complex, Mn(tpfc), exhibits high quality HFEPR spectra in frozen benzene solution, characteristic for $S = 2$. This spectroscopic result is the first for a magnetically dilute and axial ligand-free Mn^{III} corrole, so that the spin Hamiltonian parameters accurately obtained here from HFEPR are the "purest" available. However, these parameters differ minimally from those previously determined, even for Mn^{III} porphyrin complexes, indicating that all of these authentically Mn^{III} species have characteristic zfs ($D \approx -2.5 \pm 0.5$ cm^{-1} for 4- or 5-coordinate tetrapyrroles). Thus, a formally Mn^{III} tetrapyrrole that exhibits zfs well outside this range may be one with noninnocent behavior, i.e., $[Mn^{II}(P^{\bullet -})]^+$/ $[Mn^{II}(C^{\bullet 2-})]^0$. Less information is available for isoelectronic Fe^{IV}, an ion of much greater interest due to its importance in heme and nonheme iron enzymes.[122] Spin Hamiltonian parameters for Fe^{IV} in tetrapyrroles are nearly unavailable, but these have $S = 1$ ground states. In contrast, the zfs for a large number of saturated N4 macrocyclic and related coordination complexes containing the $[Fe^{IV}O]^{2+}$ (ferryl) unit have been determined. These complexes have $S = 1$ ground states and the data, chiefly Mössbauer but also from HFEPR, suggest that $D \approx +27 \pm 5$ cm^{-1}. Two formally Fe^{IV} corrole complexes were studied here by field- and frequencydomain magnetic resonance techniques, which provided complete spin Hamiltonian parameters for their $S = 1$ ground states. One of them, Fe(tpc)Ph, exhibited $D \approx 21$ cm^{-1}, which fits into this conventional description as $[Fe^{IV}(Cor^{3-})]^+$, but the other, Fe(tpc)Cl, had $D \approx 14.6$ cm^{-1}, which is far below that for any bona fide Fe^{IV} complex and suggests the alternate description, $[Fe^{III}(Cor^{\bullet 2-})]^+$. These assignments are in full agreement with previous detailed spectroscopic (chiefly XANES) studies on Fe(tpc)X, X = Cl, Ph[10] as well as computational work.[9,21] Computational studies done here, which explicitly addressed the spin Hamiltonian parameters, showed concurrence between theory and experiment. The calculated D values of $Fe(Cor^R)Ph$ (R = H or Ph meso substituents) were consistently larger, regardless of method or functional, than those calculated for $Fe(Cor^R)Cl$, although an exact match between theory and experiment was not obtained. Direct correspondence between calculated and experimental D values, even in axially symmetrical tetrapyrroles, namely Fe(tpp)X (X = F, Cl, Br, I), has proven challenging.[135] Other theoretically derived metrics such as Mulliken atomic charges and spin population support the $[Fe^{IV}(Cor^{3-})Ph]$ and $[Fe^{III}(Cor^{\bullet 2-})Cl]$ formulations, consistent with previous work,[3,10] and validated the spin Hamiltonian parameter calculations. Thus, we suggest that the zfs of formally Fe^{IV} tetrapyrroles can be used as a diagnostic of noninnocent behavior. The present study is only a first step in this direction; while the results for Mn^{III} tetrapyrroles are based on numerous examples, those for Fe^{IV} are few. In particular, full determination of zfs Fe^{IV} in porphyrin complexes, with whatever axial ligation, is sorely needed. To complete the $Fe^{III,IV}/Mn^{III,IV}$ tetrapyrrole "matrix", HFEPR and/or FD-FT THz-EPR of such formally Mn^{IV} complexes would be of interest. The zfs of bona fide Mn^{IV} coordination complexes has been determined by HFEPR,[136,137] but that of formally Mn^{IV} corroles or porphyrins is unknown, although X-band EPR of 6coordinate $Mn(tpp)X_2$ (X = N_3^-, NCO^-, CH_3O^-)[138] and of 5coordinate Mn(ttppc)X (ttppc = tris(2,4,6-triphenylphenyl) corrole trianion; X = Cl^-, HO^-)[139] suggests that the zfs is rhombic but positive and much larger than the X-band microwave quantum energy (~0.3 cm^{-1}). The zfs in formally Mn^{IV} tetrapyrroles, as in their Fe^{IV} congeners, may also be diagnostic of noninnocent behavior.

DOI: 10.1021/acs.inorgchem.9b02635
Inorg. Chem. 2020, 59, 1075−1090

ASSOCIATED CONTENT

* Supporting Information

The Supporting Information is available free of charge at https://pubs.acs.org/doi/10.1021/acs.inorgchem.9b02635.

Schemes (S2 and S2) show structures of complexes of interest, Mössbauer spectra of Fe(tpc)Cl and Fe(tpc)Ph and additional HFEPR spectra of Mn(tpfc) and Fe(tpc)Cl, quantum chemical theory (CP-DFT and CASSCF) results and discussion for iron corroles including tables of calculated values (Tables S1−S10) and MO diagrams (Figures S5−S7) (PDF)

AUTHOR INFORMATION

Corresponding Author

*E-mail: jtelser@roosevelt.edu.

ORCID

J. Krzystek: 0000-0001-6088-1936

Sebastian A. Stoian: 0000-0003-3362-7697

Andrew Ozarowski: 0000-0001-6225-9796

Mahdi M. Abu-Omar: 0000-0002-4412-1985

Abhik Ghosh: 0000-0003-1161-6364

Zachary J. Tonzetich: 0000-0001-7010-8007

Joshua Telser: 0000-0003-3307-2556

Notes

The authors declare no competing financial interest.

ACKNOWLEDGMENTS

Z.J.T. acknowledges support from the Welch Foundation (AX1772). M.M.A.-O. acknowledges support from NSF award CHE-1856753. A portion of this work was performed at the National High Magnetic Field Laboratory, which is supported by NSF Cooperative Agreement DMR-1644779 and the State of Florida. The authors are grateful to Dirk Ponwitz and Dr. Thomas Lohmiller (HZB) respectively for experimental assistance with the FD-FT THZ-EPR experiments at HZB and for help with data representation. Support for these experiments through HZB′s user program and DFG SPP 1601 is gratefully acknowledged. We thank Dr. Eckhard Bill (MPICEC, Mülheim) for helpful discussions.

REFERENCES

(1) Licoccia, S.; Paolesse, R. Metal Complexes of Corroles and Other Complexes. Struct. Bonding (Berlin) 1995, 84, 71−133.

(2) Gross, Z.; Gray, H. B. How do corroles stabilize high valent metals? Comments Inorg. Chem. 2006, 27, 61−72.

(3) Thomas, K. E.; Alemayehu, A. B.; Conradie, J.; Beavers, C. M.; Ghosh, A. The Structural Chemistry of Metallocorroles: Combined Xray Crystallography and Quantum Chemistry Studies Afford Unique Insights. Acc. Chem. Res. 2012, 45, 1203−1214.

(4) Abu-Omar, M. M. High-valent iron and manganese complexes of corrole and porphyrin in atom transfer and dioxygen evolving catalysis. Dalton Trans 2011, 40, 3435−3444.

(5) Jung, J.; Liu, S.; Ohkubo, K.; Abu-Omar, M. M.; Fukuzumi, S. Catalytic Two-Electron Reduction of Dioxygen by Ferrocene Derivatives with Manganese(V) Corroles. Inorg. Chem. 2015, 54, 4285−4291.

(6) Bougher, C. J.; Liu, S.; Hicks, S. D.; Abu-Omar, M. M. Valence Tautomerization of High-Valent Manganese(V)-Oxo Corrole Induced by Protonation of the Oxo Ligand. J. Am. Chem. Soc. 2015, 137, 14481−14487.

(7) Ghosh, A. Electronic Structure of Corrole Derivatives: Insights from Molecular Structures, Spectroscopy, Electrochemistry, and Quantum Chemical Calculations. Chem. Rev. 2017, 117, 3798−3881.

(8) Nardis, S.; Mandoj, F.; Stefanelli, M.; Paolesse, R. Metal complexes of corrole. Coord. Chem. Rev. 2019, 388, 360−405.

(9) Ganguly, S.; Ghosh, A. Seven Clues to Ligand Noninnocence: The Metallocorrole Paradigm. Acc. Chem. Res. 2019, 52, 2003−2014. (10) Ganguly, S.; Giles, L. J.; Thomas, K. E.; Sarangi, R.; Ghosh, A. Ligand Noninnocence in Iron Corroles: Insights from Optical and Xray Absorption Spectroscopies and Electrochemical Redox Potentials. Chem. - Eur. J. 2017, 23, 15098−15106.

(11) Rittle, J.; Green, M. T. Cytochrome P450 Compound I: Capture, Characterization, and C-H Bond Activation Kinetics. Science 2010, 330, 933−937.

(12) Schulz, C. E.; Rutter, R.; Sage, J. T.; Debrunner, P. G.; Hager, L. P. Mössbauer and electron paramagnetic resonance studies of horseradish peroxidase and its catalytic intermediates. Biochemistry 1984, 23, 4743−4754.

(13) Rutter, R.; Hager, L. P.; Dhonau, H.; Hendrich, M.; Valentine, M.; Debrunner, P. Chloroperoxidase compound I: electron paramagnetic resonance and Mössbauer studies. Biochemistry 1984, 23, 6809−6816.

(14) Jayaraj, K.; Gold, A.; Austin, R. N.; Ball, L. M.; Terner, J.; Mandon, D.; Weiss, R.; Fischer, J.; DeCian, A.; Bill, E.; Müther, M.; Schünemann, V.; Trautwein, A. X. Compound I and Compound II Analogues from Porpholactones. Inorg. Chem. 1997, 36, 4555−4566.

(15) Jayaraj, K.; Gold, A.; Austin, R. N.; Mandon, D.; Weiss, R.; Terner, J.; Bill, E.; Müther, M.; Trautwein, A. X. Compound I and II Analogs of a Chlorin. J. Am. Chem. Soc. 1995, 117, 9079−9080.

(16) Mandon, D.; Weiss, R.; Jayaraj, K.; Gold, A.; Terner, J.; Bill, E.; Trautwein, A. X. Models for peroxidase compound I: generation and spectroscopic characterization of new oxoferryl porphyrin π cation radical species. Inorg. Chem. 1992, 31, 4404−4409.

DOI: 10.1021/acs.inorgchem.9b02635
Inorg. Chem. 2020, 59, 1075−1090

(17) Cai, S.; Walker, F. A.; Licoccia, S. NMR and EPR Investigations of Iron Corrolates: Iron(III) Corrolate π Cation Radicals or Iron(IV) Corrolates? Inorg. Chem. 2000, 39, 3466−3478.

(18) Steene, E.; Wondimagegn, T.; Ghosh, A. Electrochemical and Electronic Absorption Spectroscopic Studies of Substituent Effects in Iron(IV) and Manganese(IV) Corroles. Do the Compounds Feature High-Valent Metal Centers or Noninnocent Corrole Ligands? Implications for Peroxidase Compound I and II Intermediates. J. Phys. Chem. B 2001, 105, 11406−11413.

(19) Steene, E.; Wondimagegn, T.; Ghosh, A. Electrochemical and Electronic Absorption Spectroscopic Studies of Substituent Effects in Iron(IV) and Manganese(IV) Corroles. Do the Compounds Feature High-Valent Metal Centers or Noninnocent Corrole Ligands? Implications for Peroxidase Compound I and II. J. Phys. Chem. B 2002, 106, 5312−5313.

(20) Zakharieva, O.; Schünemann, V.; Gerdan, M.; Licoccia, S.; Cai, S.; Walker, F. A.; Trautwein, A. X. Is the Corrolate Macrocycle Innocent or Noninnocent? Magnetic Susceptibility, Mössbauer, ^{1}H NMR, and DFT Investigations of Chloro- and Phenyliron Corrolates. J. Am. Chem. Soc. 2002, 124, 6636−6648.

(21) Ye, S.; Tuttle, T.; Bill, E.; Simkhovich, L.; Gross, Z.; Thiel, W.; Neese, F. The Electronic Structure of Iron Corroles: A Combined Experimental and Quantum Chemical Study. Chem. - Eur. J. 2008, 14, 10839−10851.

(22) Roos, B. O.; Veryazov, V.; Conradie, J.; Taylor, P. R.; Ghosh, A. Not Innocent: Verdict from Ab Initio Multiconfigurational SecondOrder Perturbation Theory on the Electronic Structure of Chloroiron Corrole. J. Phys. Chem. B 2008, 112, 14099−14102.

(23) Boca, R. Zero-field splitting in metal complexes. Coord. Chem. Rev. 2004, 248, 757−815.

(24) Telser, J. EPR Interactions−Zero-Field Splittings. In eMagRes.; John Wiley & Sons, Ltd: 2017; Vol. 6, pp 207−233.

(25) Krzystek, J.; Ozarowski, A.; Telser, J. Multi-frequency, highfield EPR as a powerful tool to accurately determine zero-field splitting in high-spin transition metal coordination complexes. Coord. Chem. Rev. 2006, 250, 2308−2324.

(26) Telser, J.; Krzystek, J.; Ozarowski, A. High-frequency and highfield electron paramagnetic resonance (HFEPR): a new spectroscopic tool for bioinorganic chemistry. JBIC, J. Biol. Inorg. Chem. 2014, 19, 297−318.

(27) Telser, J.; Ozarowski, A.; Krzystek, J. High-frequency and -field electron paramagnetic resonance of transition metal ion (d block) coordination complexes. In Electron Paramagnetic Resonance; The Royal Society of Chemistry: 2013; Vol. 23, pp 209−263.

(28) Nehrkorn, J.; Holldack, K.; Bittl, R.; Schnegg, A. Recent progress in synchrotron-based frequency-domain Fourier-transform THz-EPR. J. Magn. Reson. 2017, 280, 10−19.

(29) Schnegg, A.; Behrends, J.; Lips, K.; Bittl, R.; Holldack, K. Frequency domain Fourier transform THz-EPR on single molecule magnets using coherent synchrotron radiation. Phys. Chem. Chem. Phys. 2009, 11, 6820−6825.

(30) Krzystek, J.; Telser, J. Measuring giant anisotropy in paramagnetic transition metal complexes with relevance to singleion magnetism. Dalton Trans 2016, 45, 16751−16763.

(31) For convenience, we use the nomenclature trianion, which would be the case for the isolated, deprotonated ligand.

(32) Mn(tpfc) absent an axial ligand has not been structurally characterized, but Mn(tpfc)(κ^1-EtOAc) (i.e., axial coordination by the carbonyl oxygen of ethyl acetate from solvent; CSD code: SEVXAT) has been.

(33) Zdilla, M. J.; Abu-Omar, M. M. Mechanism of Catalytic Aziridination with Manganese Corrole: The Often Postulated HighValent Mn(V) Imido Is Not the Group Transfer Reagent. J. Am. Chem. Soc. 2006, 128, 16971−16979.

(34) Liu, H.-Y.; Mahmood, M. H. R.; Qiu, S.-X.; Chang, C. K. Recent developments in manganese corrole chemistry. Coord. Chem. Rev. 2013, 257, 1306−1333.

(35) Ganguly, S.; MCormick, L. J.; Conradie, J.; Gagnon, K. J.; Sarangi, R.; Ghosh, A. Electronic Structure of Manganese Corroles Revisited: X-ray Structures, Optical and X-ray Absorption Spectroscopies, and Electrochemistry as Probes of Ligand Noninnocence. Inorg. Chem. 2018, 57, 9656−9669.

(36) Bougher, C. J.; Abu-Omar, M. M. Lewis-Acid-assisted Hydrogen Atom Transfer to Manganese(V)-Oxo Corrole through Valence Tautomerization. ChemistryOpen 2016, 5, 522−524.

(37) Licoccia, S.; Morgante, E.; Paolesse, R.; Polizio, F.; Senge, M. O.; Tondello, E.; Boschi, T. Tetracoordinated Manganese(III) Alkylcorrolates. Spectroscopic Studies and the Crystal and Molecular Structure of (7,13-Dimethyl-2,3,8,12,17,18-hexaethylcorrolato)manganese(III). Inorg. Chem. 1997, 36, 1564−1570.

(38) Krzystek, J.; Telser, J.; Knapp, M. J.; Hendrickson, D. N.; Aromí, G.; Christou, G.; Angerhofer, A.; Brunel, L. C. High-frequency and -field electron paramagnetic resonance of high-spin manganese(III) in axially symmetric coordination complexes. Appl. Magn. Reson. 2001, 21, 571−585.

(39) Krzystek, J.; Pardi, L. A.; Brunel, L.-C.; Goldberg, D. P.; Hoffman, B. M.; Licoccia, S.; Telser, J. High-frequency and -field electron paramagnetic resonance of high-spin manganese(III) in tetrapyrrole complexes. Spectrochim. Acta, Part A 2002, 58, 1113−1127.

(40) Krzystek, J.; Telser, J. High frequency and field EPR spectroscopy of Mn(III) complexes in frozen solutions. J. Magn. Reson. 2003, 162, 454−465.

(41) Pascual-Álvarez, A.; Vallejo, J.; Pardo, E.; Julve, M.; Lloret, F.; Krzystek, J.; Armentano, D.; Wernsdorfer, W.; Cano, J. Field-Induced Slow Magnetic Relaxation in a Mononuclear Manganese(III)− Porphyrin Complex. Chem. - Eur. J. 2015, 21, 17299−17307.

(42) Tadyszak, K.; Rudowicz, C.; Ohta, H.; Sakurai, T. Electron magnetic resonance data on high-spin Mn(III; S = 2) ions in porphyrinic and salen complexes modeled by microscopic spin Hamiltonian approach. J. Inorg. Biochem. 2017, 175, 36−46.

(43) Horitani, M.; Yashiro, H.; Hagiwara, M.; Hori, H. Multifrequency and high-field EPR study of manganese(III) protoporphyrin IX reconstituted myoglobin with an S = 2 integer electron spin. J. Inorg. Biochem. 2008, 102, 781−788.

(44) Brackett, G. C.; Richards, P. L.; Caughey, W. S. Far-infrared magnetic resonance in Fe(III) and Mn(III) porphyrins, myoglobin, hemoglobin, ferrichrome A, and Fe(III) dithiocarbamates. J. Chem. Phys. 1971, 54, 4383−4401.

(45) Dugad, L. B.; Behere, D. V.; Marathe, V. R.; Mitra, S. Magnetic properties and electronic structure of manganese(III) porphyrins. Chem. Phys. Lett. 1984, 104, 353−356.

(46) Kennedy, B. J.; Murray, K. S. Magnetic Properties and ZeroField Splitting in High-Spin Manganese(III) Complexes. 2.

DOI: 10.1021/acs.inorgchem.9b02635
Inorg. Chem. 2020, 59, 1075−1090

Axially Ligated Manganese(III) Porphyrin Complexes. Inorg. Chem. 1985, 24, 1557−1560.

(47) Bendix, J.; Gray, H. B.; Golubkov, G.; Gross, Z. High-field (high-frequency) EPR spectroscopy and structural characterization of a novel manganese(III) corrole. Chem. Commun. 2000, 1957−1958.

(48) Krzystek, J.; Telser, J.; Hoffman, B. M.; Brunel, L.-C.; Licoccia, S. High-frequency and field EPR investigation of (8,12-diethyl2,3,7,13,18-hexamethylcorrolato)manganese(III). J. Am. Chem. Soc. 2001, 123, 7890−7897.

(49) Schwalbe, M.; Dogutan, D. K.; Stoian, S. A.; Teets, T. S.; Nocera, D. G. Xanthene-Modified and Hangman Iron Corroles. Inorg. Chem. 2011, 50, 1368−1377.

(50) Simkhovich, L.; Galili, N.; Saltsman, I.; Goldberg, I.; Gross, Z.
Coordination Chemistry of the Novel 5,10,15-Tris-(pentafluorophenyl)corrole: Synthesis, Spectroscopy, and Structural Characterization of Its Cobalt(III), Rhodium(III), and Iron(IV) Complexes. Inorg. Chem. 2000, 39, 2704−2705.

(51) Nardis, S.; Cicero, D. O.; Licoccia, S.; Pomarico, G.; Berionni Berna, B.; Sette, M.; Ricciardi, G.; Rosa, A.; Fronczek, F. R.; Smith, K. M.; Paolesse, R. Phenyl Derivative of Iron 5,10,15-Tritolylcorrole. Inorg. Chem. 2014, 53, 4215−4227.

(52) Vogel, E.; Will, S.; Tilling, A. S.; Neumann, L.; Lex, J.; Bill, E.; Trautwein, A. X.; Wieghardt, K. Metallocorroles with Formally Tetravalent Iron. Angew. Chem., Int. Ed. Engl. 1994, 33, 731−735.

(53) Cai, S.; Licoccia, S.; D′Ottavi, C.; Paolesse, R.; Nardis, S.; Bulach, V.; Zimmer, B.; Shokhireva, T. K.; Ann Walker, F. Chloroiron meso-triphenylcorrolates: electronic ground state and spin delocalization. Inorg. Chim. Acta 2002, 339, 171−178.

(54) Hassan, A. K.; Pardi, L. A.; Krzystek, J.; Sienkiewicz, A.; Goy, P.; Rohrer, M.; Brunel, L.-C. Ultrawide band multifrequency highfield EMR technique: a methodology for increasing spectroscopic information. J. Magn. Reson. 2000, 142, 300−312.

(55) Weil, J. A.; Bolton, J. R. Electron Paramagnetic Resonance: Elementary Theory and Practical Applications, 2nd ed.; John Wiley & Sons, Inc.: Hoboken, NJ, 2007.

(56) Neese, F. The ORCA program system. Wiley Interdisciplinary Reviews: Computational Molecular Science 2012, 2, 73−78.

(57) Frisch, M. J.; Trucks, G.W.; Schlegel, H. B.; Scuseria, G. E.; Robb, M. A.; Cheeseman, J. R.; Scalmani, G.; Barone, V.; Mennucci, B.; Petersson, G. A.; Nakatsuji, H.; Caricato, M.; Li, X.; Hratchian, H. P.; Izmaylov, A. F.; Bloino, J.; Zheng, G.; Sonnenberg, J. L.; Hada, M.; Ehara, M.; Toyota, K.; Fukuda, R.; Hasegawa, J.; Ishida, M.; Nakajima, T.; Honda, Y.; Kitao, O.; Nakai, H.; Vreven, T.; Montgomery, J. A., Jr.; Peralta, J. E.; Ogliaro, F.; Bearpark, M.; Heyd, J. J.; Brothers, E.; Kudin, K. N.; Staroverov, V. N.; Kobayashi, R.; Normand, J.; Raghavachari, K.; Rendell, A.; Burant, J. C.; Iyengar, S. S.; Tomasi, J.; Cossi, M.; Rega, N.; Millam, J. M.; Klene, M.; Knox, J. E.; Cross, J. B.; Bakken, V.; Adamo, C.; Jaramillo, J.; Gomperts, R.; Stratmann, R. E.; Yazyev, O.; Austin, A. J.; Cammi, R.; Pomelli, C.; Ochterski, J. W.; Martin, R. L.; Morokuma, K.; Zakrzewski, V. G.; Voth, G. A.; Salvador, P.; Dannenberg, J. J.; Dapprich, S.; Daniels, A. D.; Farkas, O.; Foresman, J. B.; Ortiz, J. V.; Cioslowski, J.; Fox, D. J. Gaussian 09, Revision D.01; Gaussian, Inc.: Wallingford, CT, 2009.

(58) Lee, C.; Yang, W.; Parr, R. G. Development of the ColleSalvetti correlation-energy formula into a functional of the electron density. Phys. Rev. B: Condens. Matter Mater. Phys. 1988, 37, 785−789.

(59) Wachters, A. J. H. Gaussian Basis Set for Molecular Wavefunctions Containing Third-Row Atoms. J. Chem. Phys. 1970, 52, 1033−1036.

(60) Becke, A. D. Density-functional Thermochemistry. III. The Role of Exact Exchange. J. Chem. Phys. 1993, 98, 5648−5652.

(61) Neese, F. ORCA - an ab initio, Density Functional and Semiempirical Program Package, 4.2.1; Max Planck Institut für Kohlenforschung: Mülheim an der Ruhr, Germany, 2019.

(62) Neese, F. Prediction of electron paramagnetic resonance g values using coupled perturbed Hartree−Fock and Kohn−Sham theory. J. Chem. Phys. 2001, 115, 11080−11096.

(63) Neese, F. Importance of Direct Spin−Spin Coupling and SpinFlip Excitations for the Zero-Field Splittings of Transition Metal Complexes: A Case Study. J. Am. Chem. Soc. 2006, 128, 10213− 10222.

(64) Neese, F. Calculation of the zero-field splitting tensor on the basis of hybrid density functional and Hartree-Fock theory. J. Chem. Phys. 2007, 127, 164112.

(65) Sandhoefer, B.; Neese, F. One-electron contributions to the gtensor for second-order Douglas−Kroll−Hess theory. J. Chem. Phys. 2012, 137, 094102.

(66) Schafer, A.; Horn, H.; Ahlrichs, R. Fully optimized contracted Gaussian basis sets for atoms Li to Kr. J. Chem. Phys. 1992, 97, 2571− 2577.

(67) Schafer, A.; Huber, C.; Ahlrichs, R. Fully Optimized Contracted Gaussian Basis Sets of Triple Zeta Valence Quality for Atoms Li to Kr. J. Chem. Phys. 1994, 100, 5829−5835.

(68) Ganyushin, D.; Gilka, N.; Taylor, P. R.; Marian, C. M.; Neese, F. The resolution of the identity approximation for calculations of spin-spin contribution to zero-field splitting parameters. J. Chem. Phys. 2010, 132, 144111.

(69) Aravena, D.; Atanasov, M.; Chilkuri, V. G.; Guo, Y.; Jung, J.; Maganas, D.; Mondal, B.; Schapiro, I.; Sivalingam, K.; Ye, S.; Neese, F. CASSCF Calculations in ORCA (4.2): A tutorial Introduction; Max Planck Institut für Kohlenforschung: Mülheim an der Ruhr, Germany, 2019; p 91.

(70) Krivokapic, I.; Noble, C.; Klitgaard, S.; Tregenna-Piggott, P. L. W.; Weihe, H.; Barra, A.-L. Anisotropic hyperfine interaction in the manganese(III) hexaaqua ion. Angew. Chem., Int. Ed. 2005, 44, 3613− 3616.

(71) Hagen, W. High-frequency EPR of transition ion complexes and metalloproteins. Coord. Chem. Rev. 1999, 190, 209−229.

(72) Krzystek, J.; Yeagle, G.; Park, J.-H.; Meisel, M. W.; Britt, R. D.; Brunel, L.-C.; Telser, J. High frequency and field EPR spectroscopy of tris(2,4-pentanedionato)manganese(III): investigation of solid-state versus solution Jahn-Teller effects. Inorg. Chem. 2003, 42, 4610−4618. (73) Campbell, K. A.; Yikilmaz, E.; Grant, C. V.; Gregor, W.; Miller, A.-F.; Britt, R. D. Parallel Polarization EPR Characterization of the Mn(III) Center of Oxidized Manganese Superoxide Dismutase. J. Am. Chem. Soc. 1999, 121, 4714−4715.

(74) Campbell, K. A.; Lashley, M. R.; Wyatt, J. K.; Nantz, M. H.; Britt, R. D. Dual-Mode EPR Study of Mn(III) Salen and the Mn(III) Salen-Catalyzed Epoxidation of cis-β-Methylstyrene. J. Am. Chem. Soc. 2001, 123, 5710−5719.

DOI: 10.1021/acs.inorgchem.9b02635
Inorg. Chem. 2020, 59, 1075−1090

(75) Gupta, R.; Taguchi, T.; Borovik, A. S.; Hendrich, M. P. Characterization of Monomeric $Mn^{II/III/IV}$–Hydroxo Complexes from X- and Q-Band Dual Mode Electron Paramagnetic Resonance (EPR) Spectroscopy. Inorg. Chem. 2013, 52, 12568−12575.

(76) The study by Ye et al. reported Mössbauer parameters for a number of corroles of general type Fe(triaryl)X as well as for some corresponding porphyrin complexes; their Table 1 is very instructive.[21]

(77) Bill, E.; Schünemann, V.; Trautwein, A. X.; Weiss, R.; Fischer, J.; Tabard, A.; Guilard, R. Mössbauer investigations of the hexachlorantimonate salt of the phenyliron 2,3,7,8,12,13,17,18octaethyl-5,10,15,20-tetraphenylporphyrinate, [Fe(oetpp)Ph]$SbCl_6$ and X-ray structure of the phenyliron(III) precursor Fe(III)(oetpp)Ph. Inorg. Chim. Acta 2002, 339, 420−426.

(78) Pardi, L. A.; Krzystek, J.; Telser, J.; Brunel, L.-C. Multifrequency EPR spectra of molecular oxygen in solid air. J. Magn. Reson. 2000, 146, 375−378.

(79) Stoll, S.; Schweiger, A. EasySpin, a comprehensive software package for spectral simulation and analysis in EPR. J. Magn. Reson. 2006, 178, 42−55.

(80) Nehrkorn, J.; Telser, J.; Holldack, K.; Stoll, S.; Schnegg, A. Simulating Frequency-Domain Electron Paramagnetic Resonance: Bridging the Gap between Experiment and Magnetic Parameters for High-Spin Transition-Metal Ion Complexes. J. Phys. Chem. B 2015, 119, 13816−13824.

(81) Abragam, A.; Bleaney, B. Electron Paramagnetic Resonance of Transition Ions (Oxford Classic Texts in the Physical Sciences); Oxford University Press: Oxford, UK, 2012.

(82) Griffith, J. S. The Theory of Transition-Metal Ions; Cambridge University Press: Cambridge, UK, 1964.

(83) Krzystek, J.; Telser, J.; Pardi, L. A.; Goldberg, D. P.; Hoffman, B. M.; Brunel, L.-C. High-frequency and -field electron paramagnetic resonance of high-spin manganese(III) in porphyrinic complexes. Inorg. Chem. 1999, 38, 6121−6129.

(84) Tregenna-Piggott, P. L. W.; Weihe, H.; Barra, A.-L. High-field, multifrequency EPR study of the $[Mn(OH_2)_6]^{3+}$ cation: influence of π-bonding on the ground state zero-field-splitting parameters. Inorg. Chem. 2003, 42, 8504−8508.

(85) Krzystek, J.; Yeagle, G. J.; Park, J.-H.; Britt, R. D.; Meisel, M. W.; Brunel, L.-C.; Telser, J. High-Frequency and -Field EPR Spectroscopy of Tris(2,4-pentanedionato)manganese(III): Investigation of Solid-State versus Solution Jahn−Teller Effects. Inorg. Chem. 2009, 48, 3290−3291.

(86) Duboc, C.; Ganyushin, D.; Sivalingam, K.; Collomb, M.-N.; Neese, F. Systematic Theoretical Study of the Zero-Field Splitting in Coordination Complexes of Mn(III). Density Functional Theory versus Multireference Wave Function Approaches. J. Phys. Chem. A 2010, 114, 10750−10758.

(87) Maurice, R.; de Graaf, C.; Guihery, N. Magnetostructural relations from a combined ab initio and ligand field analysis for the nonintuitive zero-field splitting in Mn(III) complexes. J. Chem. Phys. 2010, 133, 084307.

(88) Shova, S.; Vlad, A.; Cazacu, M.; Krzystek, J.; Bucinsky, L.; Breza, M.; Darvasiova, D.; Rapta, P.; Cano, J.; Telser, J.; Arion, V. B. A five-coordinate manganese(III) complex of a salen type ligand with a positive axial anisotropy parameter D. Dalton Trans 2017, 46, 11817−11829.

(89) Krzystek, J.; Telser, J.; Li, J.; Subramanian, M. A. Magnetic Properties and Electronic Structure of Manganese-Based Blue Pigments: A High-Frequency and -Field EPR Study. Inorg. Chem. 2015, 54, 9040−9045.

(90) There are 6-coordinate Mn^{III} complexes with light-atom ligands wherein, for various reasons, there is axial compression and D > 0.[88,91,92]

(91) Scheifele, Q.; Riplinger, C.; Neese, F.; Weihe, H.; Barra, A.-L.; Juranyi, F.; Podlesnyak, A.; Tregenna-Piggott, P. L. W. Spectroscopic and Theoretical Study of a Mononuclear Manganese(III) Complex Exhibiting a Tetragonally Compressed Geometry. Inorg. Chem. 2008, 47, 439−447.

(92) Romain, S.; Duboc, C.; Neese, F.; Riviere, E.; Hanton, L. R.; Blackman, A. G.; Philouze, C.; Lepretre, J.-C.; Deronzier, A.; Collomb, M.-N. An Unusual Stable Mononuclear Mn^{III} Bisterpyridine Complex Exhibiting Jahn−Teller Compression: Electrochemical Synthesis, Physical Characterisation and Theoretical Study. Chem. - Eur. J. 2009, 15, 980−988.

(93) An exception in the 6-coordinate case is when the tetragonally elongated axial ligand(s) are heavy atoms, in particular iodine, wherein spin delocalization onto the iodido ligands leads to spin− orbit coupling (SOC) contributions from iodine 5p electrons that makes a simple $3d^4$ LFT model unsuitable. In this case, as seen in $[Mn^{III}(cyclam)I_2]I$ (cyclam = 1,4,8,11-tetraazacyclotetradecane), the zfs is positive.[94]

(94) Mossin, S.; Weihe, H.; Barra, A.-L. Is the Axial Zero-Field Splitting Parameter of Tetragonally Elongated High-Spin Manganese(III) Complexes Always Negative? J. Am. Chem. Soc. 2002, 124, 8764−8765.

(95) This phenomenon may be responsible for the zfs of Mn(oep)Br being relatively small in magnitude. Mn(oep)I has not been qualitatively analyzed, but its zfs is likely even smaller in magnitude: preliminary HFEPR studies and the fact that it gives a frozen solution X-band signal suggest Mn(oep)I has $|D| \sim 0.1$ cm^{-1}.[38]

(96) Harvey, J. D.; Ziegler, C. J.; Telser, J.; Ozarowski, A.; Krzystek, J. High-frequency and -field EPR investigation of a manganese(III) Nconfused porphyrin complex, $[Mn(NCTPP)(py)_2]$. Inorg. Chem. 2005, 44, 4451−4453.

(97) Busby, C. A.; Dinello, R. K.; Dolphin, D. A Convenient Preparation of meso-Tetra(4-sulfonatophenyl)porphyrin. Can. J. Chem. 1975, 53, 1554−1555.

(98) Jiang, X.; Gros, C. P.; Chang, Y.; Desbois, N.; Zeng, L.; Cui, Y.; Kadish, K. M. Tetracationic and Tetraanionic Manganese Porphyrins: Electrochemical and Spectroelectrochemical Characterization. Inorg. Chem. 2017, 56, 8045−8057.

(99) Yu, N.-T.; Tsubaki, M. Resonance Raman spectra of manganese myoglobin and its azide complex. Assignment of a new charge-transfer band to azide (π) → porphyrin (π*) transition. Biochemistry 1980, 19, 4647−4653.

(100) Groves, J. T.; Quinn, R.; McMurry, T. J.; Nakamura, M.; Lang, G.; Boso, B. Preparation and Characterization of a Dialkoxyiron(IV) Porphyrin. J. Am. Chem. Soc. 1985, 107, 354−360.

(101) Boaz, N. C.; Bell, S. R.; Groves, J. T. Ferryl Protonation in Oxoiron(IV) Porphyrins and Its Role in Oxygen Transfer. J. Am. Chem. Soc. 2015, 137, 2875−2885.

(102) Shan, X.; Que, L., Jr. High-valent nonheme iron-oxo species in biomimetic oxidations. J. Inorg. Biochem. 2006, 100, 421−433.

DOI: 10.1021/acs.inorgchem.9b02635
Inorg. Chem. 2020, 59, 1075−1090

(103) Decker, A.; Rohde, J.-U.; Klinker, E. J.; Wong, S. D.; Que, L.; Solomon, E. I. Spectroscopic and Quantum Chemical Studies on Low-Spin Fe^{IV}=O Complexes: Fe-O Bonding and Its Contributions to Reactivity. J. Am. Chem. Soc. 2007, 129, 15983−15996.

(104) Que, L., Jr. The Road to Non-Heme Oxoferryls and Beyond. Acc. Chem. Res. 2007, 40, 493−500.

(105) England, J.; Guo, Y.; Farquhar, E. R.; Young, V. G., Jr.; Münck, E.; Que, L., Jr. The Crystal Structure of a High-Spin Oxoiron(IV) Complex and Characterization of Its Self-Decay Pathway. J. Am. Chem. Soc. 2010, 132, 8635−8644.

(106) McDonald, A. R.; Que, L., Jr. High-valent nonheme iron-oxo complexes: Synthesis, structure, and spectroscopy. Coord. Chem. Rev. 2013, 257, 414−428.

(107) Puri, M.; Que, L., Jr. Toward the Synthesis of More Reactive S = 2 Non-Heme Oxoiron(IV) Complexes. Acc. Chem. Res. 2015, 48, 2443−2452.

(108) Krzystek, J.; England, J.; Ray, K.; Ozarowski, A.; Smirnov, D.; Que, L., Jr.; Telser, J. Determination by High-Frequency and -Field EPR of Zero-Field Splitting in Iron(IV) Oxo Complexes: Implications for Intermediates in Nonheme Iron Enzymes. Inorg. Chem. 2008, 47, 3483−3485.

(109) Bucinsky, L.; Rohde, G. T.; Que, L., Jr.; Ozarowski, A.; Krzystek, J.; Breza, M.; Telser, J. HFEPR and Computational Studies on the Electronic Structure of a High-Spin Oxidoiron(IV) Complex in Solution. Inorg. Chem. 2016, 55, 3933−3945.

(110) Rasheed, W.; Draksharapu, A.; Banerjee, S.; Young, V. G., Jr.; Fan, R.; Guo, Y.; Ozerov, M.; Nehrkorn, J.; Krzystek, J.; Telser, J.; Que, L., Jr. Crystallographic Evidence for a Sterically Induced Ferryl Tilt in a Non-Heme Oxoiron(IV) Complex that Makes it a Better Oxidant. Angew. Chem., Int. Ed. 2018, 57, 9387−9391.

(111) Solomon, E. I.; Light, K. M.; Liu, L. V.; Srnec, M.; Wong, S. D. Geometric and Electronic Structure Contributions to Function in Non-heme Iron Enzymes. Acc. Chem. Res. 2013, 46, 2725−2739.

(112) Shaik, S.; Kumar, D.; de Visser, S. P.; Altun, A.; Thiel, W. Theoretical perspective on the structure and mechanism of cytochrome P450 enzymes. Chem. Rev. 2005, 105, 2279−2328.

(113) Usharani, D.; Janardanan, D.; Li, C.; Shaik, S. A Theory for Bioinorganic Chemical Reactivity of Oxometal Complexes and Analogous Oxidants: The Exchange and Orbital-Selection Rules. Acc. Chem. Res. 2013, 46, 471−482.

(114) Barefield, E. K. Coordination chemistry of N-tetraalkylated cyclam ligands A status report. Coord. Chem. Rev. 2010, 254, 1607− 1627.

(115) Sastri, C. V.; Lee, J.; Oh, K.; Lee, Y. J.; Lee, J.; Jackson, T. A.; Ray, K.; Hirao, H.; Shin, W.; Halfen, J. A.; Kim, J.; Que, L., Jr.; Shaik, S.; Nam, W. Axial ligand tuning of a nonheme iron(IV)−oxo unit for hydrogen atom abstraction. Proc. Natl. Acad. Sci. U. S. A. 2007, 104, 19181−19186.

(116) Jackson, T. A.; Rohde, J.-U.; Seo, M. S.; Sastri, C. V.; DeHont, R.; Stubna, A.; Ohta, T.; Kitagawa, T.; Münck, E.; Nam, W.; Que, L. Axial Ligand Effects on the Geometric and Electronic Structures of Nonheme Oxoiron(IV) Complexes. J. Am. Chem. Soc. 2008, 130, 12394−12407.

(117) Bukowski, M. R.; Koehntop, K. D.; Stubna, A.; Bominaar, E. L.; Halfen, J. A.; Münck, E.; Nam, W.; Que, L., Jr. A Thiolate-Ligated Nonheme Oxoiron(IV) Complex Relevant to Cytochrome P450. Science 2005, 310, 1000−1002.

(118) Thibon, A.; England, J.; Martinho, M.; Young, V. G., Jr.; Frisch, J. R.; Guillot, R.; Girerd, J.-J.; Münck, E.; Que, L., Jr.; Banse, F. Proton- and Reductant-Assisted Dioxygen Activation by a Nonheme Iron(II) Complex to Form an Oxoiron(IV) Intermediate. Angew. Chem., Int. Ed. 2008, 47, 7064−7067.

(119) Grapperhaus, C. A.; Mienert, B.; Bill, E.; Weyhermuller, T.; Wieghardt, K. Mononuclear (Nitrido)iron(V) and (Oxo)iron(IV) Complexes via Photolysis of [(cyclam-acetato)$Fe^{III}(N_3)]^+$ and Ozonolysis of [(cyclam-acetato)$Fe^{III}(O_3SCF_3)]^+$ in Water/Acetone Mixtures. Inorg. Chem. 2000, 39, 5306−5317.

(120) Chanda, A.; Shan, X.; Chakrabarti, M.; Ellis, W. C.; Popescu, D. L.; Tiago de Oliveira, F.; Wang, D.; Que, L.; Collins, T. J.; Münck, E.; Bominaar, E. L. (TAML)Fe^{IV}=O Complex in Aqueous Solution: Synthesis and Spectroscopic and Computational Characterization. Inorg. Chem. 2008, 47, 3669−3678.

(121) Ray, K.; England, J.; Fiedler, A. T.; Martinho, M.; Münck, E.; Que, L., Jr. An Inverted and More Oxidizing Isomer of $[Fe^{IV}(O)(tmc)(NCCH_3)]^{2+}$. Angew. Chem., Int. Ed. 2008, 47, 8068−8071.

(122) Ghosh, A. High-valent iron intermediates in biology. J. Inorg. Biochem. 2006, 100, 419−420.

(123) Collins, T. J. TAML Oxidant Activators: A New Approach to the Activation of Hydrogen Peroxide for Environmentally Significant Problems. Acc. Chem. Res. 2002, 35, 782−790. (124) Ghosh, A.; Mitchell, D. A.; Chanda, A.; Ryabov, A. D.; Popescu, D. L.; Upham, E. C.; Collins, G. J.; Collins, T. J. Catalase− Peroxidase Activity of Iron(III)−TAML Activators of Hydrogen Peroxide. J. Am. Chem. Soc. 2008, 130, 15116−15126.

(125) There is no $[Fe(O)(tmc)]^{2+}$ absent an axial ligand, for direct comparison with $[Fe(O)B^*]^{2-}$, although X = MeCN is a relatively weak donor.

(126) Fe(dmhec)Ph has D = 20 cm^{-1}, lower still, but determination of zfs from magnetic susceptibility is fraught with unreliability.[30]

(127) As mentioned in Table 3 (note h), spin-coupling coefficients (see Boca, Table 14, eqs 3.26, 3.27)[23] for $S_A = 1/2$, $S_B = 3/2$, would give $|D_{S=1}| = 14$ cm^{-1} only if $|D_{Fe}| = 9.35$ cm^{-1}; $|D_{Fe}| = 28$ cm^{-1} would give $|D_{S=1}| = 14$ cm^{-1}. Simultaneous extraction of exchange coupling and single ion zfs from magnetic susceptibility is risky, but Ye et al. did fit their magnetometry data with $D_{Fe} = 9.5(2)$ cm^{-1},[21] which range would give exactly the observed overall D for Fe(tpc)Cl. Nevertheless, we have no bona fide S = 3/2 Fe_{III} tetrapyrrole from which to obtain a D value. There appears to be a single such complex in the literature, $Fe(tpp)(FSbF_5)\cdot C_6H_5F$,[128] but its magnetic susceptibility and Mössbauer data were not analyzed using an S = 3/2 spin Hamiltonian, so it cannot be used for direct comparison, as already noted by Ye et al. (see their footnote 25).[21]

(128) Gupta, G. P.; Lang, G.; Reed, C. A.; Shelly, K.; Scheidt, W. R. Susceptibility and Mössbauer study of an antiferromagnetically coupled admixed-intermediate spin state in $Fe(TPP)(FSbF_5)\cdot C_6H_5F$. J. Chem. Phys. 1987, 86, 5288−5293.

(129) Duboc, C. Determination and prediction of the magnetic anisotropy of Mn ions. Chem. Soc. Rev. 2016, 45, 5834−5847.

(130) Boyd, R. J. A quantum mechanical explanation for Hund's multiplicity rule. Nature 1984, 310, 480−481.

(131) McGarvey, B. R. Electron Spin Resonance of Transition Metal Complexes. In Transition Metal Chemistry; Carlin, R. L., Ed.; Marcel Dekker: New York, 1966; pp 89−201.

DOI: 10.1021/acs.inorgchem.9b02635
Inorg. Chem. 2020, 59, 1075−1090

(132) McGarvey, B. R. Survey of ligand field parameters of strong field d^5 complexes obtained from the g matrix. Coord. Chem. Rev. 1998, 170, 75−92.

(133) Oosterhuis, W. T.; Lang, G. Magnetic properties of the t_{2g}^4 configuration in low symmetry crystal fields. J. Chem. Phys. 1973, 58, 4757−4765.

(134) See Oosterhius and Lang Appendix B, eqs B1 and B2.[133]

(135) Stavretis, S. E.; Atanasov, M.; Podlesnyak, A. A.; Hunter, S. C.; Neese, F.; Xue, Z.-L. Magnetic Transitions in Iron Porphyrin Halides by Inelastic Neutron Scattering and Ab Initio Studies of Zero-Field Splittings. Inorg. Chem. 2015, 54, 9790−9801.

(136) Duboc, C.; Collomb, M.-N. Multifrequency high-field EPR investigation of a mononuclear manganese(IV) complex. Chem. Commun. 2009, 2715−2717.

(137) Zlatar, M.; Gruden, M.; Vassilyeva, O. Y.; Buvaylo, E. A.; Ponomarev, A. N.; Zvyagin, S. A.; Wosnitza, J.; Krzystek, J.; GarciaFernandez, P.; Duboc, C. Origin of the Zero-Field Splitting in Mononuclear Octahedral Mn^{IV} Complexes: A Combined Experimental and Theoretical Investigation. Inorg. Chem. 2016, 55, 1192− 1201.

(138) Camenzind, M. J.; Hollander, F. J.; Hill, C. L. Synthesis, characterization, and ground electronic state of the unstable monomeric manganese(IV) porphyrin complexes diazido- and bis(isocyanato)(5,10,15,20-tetraphenylporphinato)manganese(IV). Crystal and molecular structure of the bis(isocyanato) complex. Inorg. Chem. 1983, 22, 3776−3784.

(139) Zaragoza, J. P. T.; Siegler, M. A.; Goldberg, D. P. A Reactive Manganese(IV)−Hydroxide Complex: A Missing Intermediate in Hydrogen Atom Transfer by High-Valent Metal-Oxo Porphyrinoid Compounds. J. Am. Chem. Soc. 2018, 140, 4380−4390.

DOI: 10.1021/acs.inorgchem.9b02635
Inorg. Chem. 2020, 59, 1075−1090